J Seismol
https://doi.org/10.1007/s10950-025-10320-0

RESEARCH

Local amplification assessment supported by geostatistical analysis and geomodelling of geophysical data for the Anse-à-Veau region, Haiti

Valmy Dorival · Hans-Balder Havenith · Kelly Guerrier · Sophia Ulysse · Dominique Boisson

Received: 17 January 2025 / Accepted: 21 July 2025

Abstract Local amplification is an important factor when assessing local earthquake ground motion in an area covered by soft sedimentary deposit (lithological site effects), 2D basins and/or marked by the presence of hills or mountains (topographical site effects). In the present study, we propose to estimate the local ground motion linked to these site effects in Anse-à-Veau, a municipality in the Nippes Department of Haiti. This region was also affected by intense seismic shaking during the M 7.2 Nippes earthquake in August 2021, and the numerous aftershocks. The surveys have been carried out during the measurement campaigns in 2021, 2022 and 2023, and include ambient noise and earthquake recordings, seismic surveys as well as electrical resistivity measurements along profiles. The two first ones were processed, respectively, in terms of horizontal to vertical spectral ratios and standard spectral ratios, the seismic tests both as seismic refraction tomography and by multichannel surface wave analysis and the last measurements as electrical resistivity tomography. In total, more than 150 ambient noise recordings, 22 seismic profiles and 8 electric profiles have been completed. All related results were then compiled within one multi-data 3D geomodel and submitted to a spatial analysis by applying a conditional geostatistical simulation which is expected to take advantage of the relationships between the different type of seismic data in order to better estimate the potential site effects in the study area. The site amplification parameters are then used to compute local ground motion for the 2021 Nippes Earthquake at Anse-à-Veau using Next Generation Attenuation.

Keywords Geostatistics · Site effects · Multi-geophysics · Geomodelling · Local ground motion

V. Dorival (✉) · H.-B. Havenith
Department of Geology, University of Liege, Liège, Belgium
e-mail: valmy.dorival@uliege.be

V. Dorival · K. Guerrier · S. Ulysse · D. Boisson
URGéo, Faculty of Sciences, State University of Haiti, Port-Au-Prince, Haiti

1 Introduction

The waves that propagate through the soil during a seismic event undergo multiple transformations related to the crossed environments. Generally, the ground motion and the damage to buildings decrease as one moves away from the epicentre of the earthquake, because the amplitude of the seismic waves decreases with the distance according to the phenomenon of attenuation (Aki and Richards 2002). However, the seismic movements recorded on the ground may be affected by the local morphological and lithological conditions. Related so-called site effects can strongly increase the seismic movements in regions covered by soft soils and deep sediments, such as lakebeds or alluvial plains, 2D basins (lateral effects

Published online: 01 August 2025

of sediment-filled valleys) and/or marked by a hilly or mountainous topography.

The soil composition is one of the most significant factors influencing the site effects. Soft soils or unconsolidated sediments have a lower shear-wave velocity compared to hard rock, which leads to slower propagation of seismic waves and increased shaking at the surface (Borcherdt and Gibbs 1976; Bard and Bouchon 1980; Bowden and Tsai 2017). Topographical features, such as hills, valleys, and ridges, can also significantly affect seismic wave propagation. Seismic waves traveling up a slope can be amplified, while those traveling downhill may experience focusing, concentrating seismic energy in certain areas (Geli et al. 1988; Zhou 2018). These local effects have been observed in numerous historical earthquakes including the 1985 Mexico earthquake and the 1999 Kocaeli earthquake in Turkey (Bard et al. 1988; Homan and Eastwood 2001).

After the 2010 Haiti earthquake, several studies have been carried out for the regional and local hazard assessment in the capital Port-au-Prince (Bertil et al. 2013; St-Fleur et al. 2016; Ulysse et al. 2018a, b) and Fonds-Parisien, 37 km to the west of Port-au-Prince (Ulysse et al. 2021). These studies show that a lot of damage observed during the 2010 earthquake can be explained by the geological and morphological conditions of the local ground. The damage observed in some areas of the southern peninsula of Haiti after the M = 7.2 Nippes earthquake and related aftershocks in August 2021 (Calais et al. 2022a, b) can be also explained by these local effects. The present study actually aims at assessing the site effects supported by geomodelling in combination with geostatistical analysis of seismic data for Anse-à-Veau, a municipality in the Nippes Department that had been hit by the 2021 earthquake.

The process of seismic hazard assessment requires then both regional and local factors to provide a more accurate prediction of the risk. The regional assessment is typically based on regional tectonic settings, fault lines and historical earthquake data (Frankel 1995). By integrating the local effects, the assessment provides a more realistic understanding of the risk which is very important in urban areas with concentrated infrastructure (de Risi et al. 2019).

The surveys carried out at Anse-à-Veau include ambient noise and earthquake recordings, seismic tests as well as electrical resistivity measurements along profiles. The geostatistical analysis applied to these data is expected to take advantage of the spatial relationships between the different type of seismic data and reproduce the local changes of the site effects phenomenon via the coregionalization modelling and conditional simulation; visualisation of those changes is then also supported by 3D geomodelling. Indeed, the geostatistical technique became very popular over the past 20 years in general geosciences and has various applications, such as interpolation between scalar values, stress ellipticity (Mukul 1998), soil properties (Bourennane 1997) or geophysical prospecting (Bourges et al. 2012). Here, we try to take benefit of these capabilities to improve the local seismic hazard assessment in Haiti.

2 Seismotectonic context and study area

2.1 Seismotectonic context

Haiti is marked by a very high seismic hazard as it is located in the tectonic context (Fig. 1a) marked by the frontal subduction of the North American plate beneath the Caribbean plate in the north and the Muertos Trough with characteristics of a subduction zone off the southern coasts (Ali et al. 2008; Frankel et al. 2011). The island is crossed by two major strike-slip faults, the Septentrional and Enriquillo Plantain Garden faults in the northern and southern parts respectively, and by poorly known thrust faults such as the Matheux-Neiba Fault in the middle part of the island (DeMets et al. 2000; Mann et al. 2002; Calais et al. 2002).

The study area belongs to the geographic and structural set of the southern peninsula (Fig. 1b) formed by the two southern mountain ranges of Haiti: Massif de la Hotte and Massif de la Selle. The peninsula has an E-W general direction and includes a succession of faulted anticlines from Massif de la Hotte in the west to Massif de la Selle in the east (BME 2005). The Enriquillo Plantain Garden Fault (EPGF) crosses this peninsula in the same direction at a few kilometres in the south of the study area. It has been recognized as a major tectonic feature with a long history of major earthquakes (Scherer 1912; Ali et al. 2008; Bakun et al. 2012).

The EPGF has a slip rate of 7 ± 2 mm yr^{-1} with a left-lateral strike-slip motion according to the

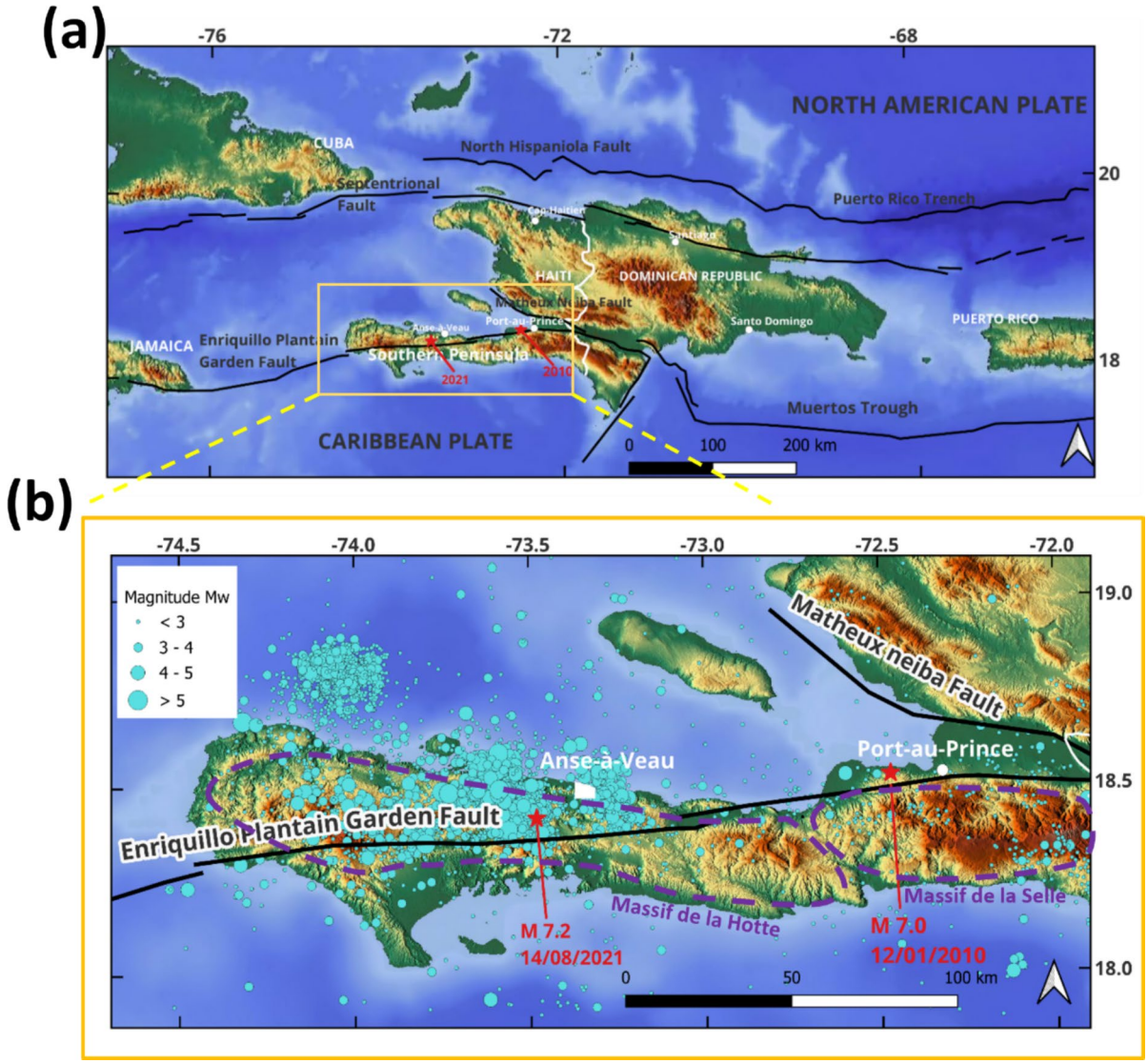

Fig. 1 (**a**) Seismotectonic context of Hispaniola Island (Haiti and Dominican Republic) with the main active faults in black lines and the two recent major earthquakes in red stars (Calais et al. 2022a, b; Bakun et al. 2012; Frankel et al. 2011). (**b**) Seismic activity (represented by the cyan dots with the size as magnitude) recorded in the southern peninsula from 2019 to 2023 by the platform *Ayiti Séismes* (https://ayiti.unice.fr/ayiti-seismes/)

interseismic plate coupling and strain partitioning in the Northeastern Caribbean (in which the EPGF system was modelled as a single vertical fault) by Manaker et al. (2008). The analysis of GPS and InSAR data by Calais et al. (2010) provides a 5 ± 1 mm yr^{-1} of transpression, combining left-lateral strike-slip and 2 ± 1 mm yr^{-1} of reverse slip for the EPGF. In the post-2010 earthquake analysis, the fault system was modelled as a single north-dipping fault since the spatial density of the GPS network was not sufficient to model the multi-fault EPGF system complexities revealed by the 2010 earthquake.

The historical earthquakes of 1701, 1751 and 1770 are thought to have occurred in the EPGF system (Scherer 1912; Ali et al. 2008; Bakun et al. 2012). The 8 April 1860 earthquake with a magnitude of 6.2 to 6.5 (Scherer 1912; Woodring et al. 1924) might have occurred outside the main trace of the EPGF on

a secondary structure, probably offshore (Bakun et al. 2012). The 12 January 2010 earthquake is now also considered to have occurred outside the main trace of the EPGF, on an unmapped north-dipping fault in the EPGF system, the Léogane Fault, according to fault modelling of coseismic deformation measured with GPS instruments and interferometric synthetic aperture radar (Calais et al. 2010). The studies completed after the main earthquake for aftershocks locations and fault geometry (Douilly et al. 2013; de Lépinay et al. 2011) show that the rupture was complex, which suggests that other structures might have been involved.

Locations of the epicentres of the historical seismic events near Anse-à-Veau could not be precisely determined and are based on current knowledge of the regional geology and active faults, as well as damage reports (Scherer 1912; Flores et al. 2012). The first reported seismic event is the 8 April 1860 earthquake with a tsunami observed along the coast. From 1909 to 1922, several strong shakings were felt at Anse-à-Veau. In October 1952, an earthquake of intensity IX and magnitude Ms = 5.9, located at a depth of 24 km, was felt in Anse-à-Veau. The shakings also occurred in January and February 1953 but were considered like probable aftershocks of the earthquake of October 1952 (Flores et al. 2012). The reports suggest that the distribution of the damage observed was related to the local conditions of the soil.

The area of Anse-à-Veau experienced a certain quiet period after the October 1952 earthquake and the aftershocks of 1953 (Flores et al. 2012). From the year 2015, the Technical Unit of Seismology (UTS) of Bureau of Mines and Energy (BME) has started recording weak to moderate earthquakes in that area, which did not produce any damage but created great panic among the people. In April 2021, a first moderate earthquake has been recorded near the area. The quake has also been felt by many people but did neither cause significant damage.

The 14 August 2021 earthquake is the most recent major event in the western part of the peninsula; it was was felt throughout the whole country as well as in the Dominican Republic and Cuba. The mainshock had a moment magnitude (*Mw*) of 7.2 with an optimal centroid source depth at 6 km and a source mechanism that combines strike-slip and reverse faulting (Calais et al. 2022a, b). It presents the same aftershocks distribution and coseismic slip north of the EPGF like the 12 January 2010 earthquake, starting with a significant component of reverse faulting motion on an eastern segment, which propagated westward with later mostly strike-slip motion (Calais et al. 2022a).

2.2 Geology of the study area

The geology of the study area (Fig. 2b) is made of sedimentary rocks as described by the regional geological map of Haiti (*Carte géologique d'Haïti au 1/250 000ème, Bureau des Mines et de l'Energie*, BME 2005). The oldest formations date back to the upper Cretaceous and are characterized by massive pelagic limestone (**Cs** on the map) from the Senonian and stratified or massive pelagic limestones (**Ep** on the map) from the upper Paleocene to lower and middle Eocene. The Paleocene and Eocene series generally form the sides of the anticlines which are mainly made of formations from the upper Cretaceous in several parts of Massif de la Hotte in the southern peninsula.

The recent formations are of Quaternary age. They are represented either by alluvial material (**Qa** on the map) along *Riviere Brossard* (the river that crosses the study area, Fig. 2c), around the pond, and at *La Basse Ville* (the lower town), in the western part of the town of Anse-à-Veau (Fig. 2c), or by reef limestones (**Qc** on the map) beneath *La Haute Ville* (the upper town) and in the easternmost portion of the study area (Fig. 2c) due to a rapid uplift of the island in the Quaternary.

The alluvium is made of clays and sands deposits around the river and the pond. In the westside, they can be related to an erosion of the northern slope of the mountain. The soil becomes lateritic and finer in some parts at the south of *La Haute Ville* and can be related to a thicker unconsolidated clay deposit. The contact between *La Haute Ville* and *La Basse Ville* is formed by some sand quarries and marly limestones with variable clay content in the S–N direction.

The town of Anse-à-Veau was not strongly affected by the 2021 event or the aftershocks like the bigger cities of Les Cayes and Jeremie of the Sud and Grand-Anse Departments (Fig. 2); the damage observed at Anse-à-Veau was mainly concentrated at *La Basse Ville* built on the Quaternary alluvium along the river (*Rivière Brossard*), while *La Haute Ville* built on the reef limestone was slightly affected. These observations are very consistent with the ones in the reports

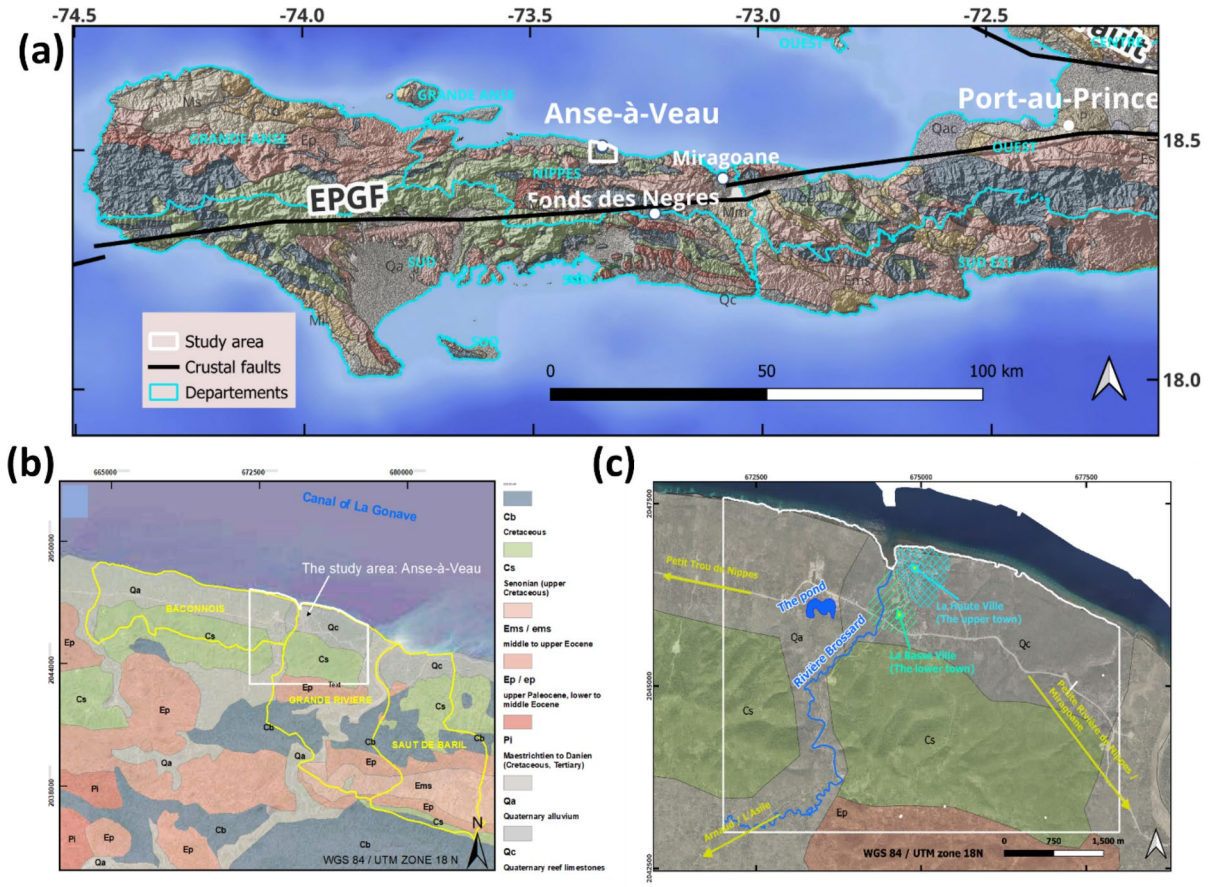

Fig. 2 (**a**) The geology of the southern peninsula from the current Haitian geological map with the Enriquillo Plantain Garden Fault (EPGF). (**b**) The geology of Anse-à-Veau with its three rural sections in yellow. (**c**) The town of Anse-à-Veau with the location of *La Haute Ville*, *La Basse Ville*, *Rivière Brossard*, the pond and the three main exits with yellow arrows

of the historical earthquakes (Scherer 1912; Flores et al. 2012). To explain these differences of observed seismic shaking effects, a geophysical-seismological investigation has been organised using the following methods.

3 Methods

3.1 Ambient noise HVSR measurements

The ambient noise HVSR (horizontal-to-vertical spectral ratio) measurements became popular after some Japanese publications (Nakamura and Saito 1983) and are sometimes referred to as the Nakamura method or Quasi Transfer Spectrum (Nakamura 1989, 2000, 2009), but are now more widely called HVSR method because it consists in dividing the spectrum of the horizontal components by the spectrum of the vertical component of ambient noise or earthquake motions (Bard 1999; Bonnefoy-Claudet et al. 2006; Chatelain et al. 2007). Currently, the earthquake hazard research community recognizes the potential of this method to give a correct estimate of the natural frequency of a site (SESAME 2004) although the theoretical background of this technique is not clear.

The current method is based on the analysis of microtremor or ambient noise as the name suggests. From the recording of the ambient noise, the HVSR (or H/V ratio) is calculated, which reflects the relative amplification of the horizontal components of the shaking with respect to the vertical one. The H/V ratio makes it possible to obtain a pseudo transfer function at the point of measurement. The peak

presented by the H/V curve provides a good estimate of the S-waves resonance frequency (and therefore that of the ground) at plus or minus 20% (for 1D structures). In contrast, the corresponding amplitude systematically underestimates the amplitude of the transfer function (SESAME 2004). It should therefore be considered as a relative value to be compared with other measurement sites.

In the case of a soft 1D sedimentary layer (having a strong impedance contrast with the bedrock), we can relate the thickness of the layer h to its fundamental resonance frequency f_0 by the expression:

$$f_0 = \frac{V_S}{4h}$$

with h: average thickness of the soft layer,

Vs: average velocity of propagation of S-waves in the soft layer,

f_0: fundamental resonance frequency of the soft layer.

The ambient noise measurements were carried out by an 'all-in-one' station including both a sensor and a digitizer: the Tromino. According to the manufacturer (the Italian company Micromed), the bandwidth of the sensor works on the following frequency range: 0.1–1024 Hz.

3.2 Earthquake recordings

The earthquake recordings were mainly used in our case for the application of the Standard Spectral Ratio (SSR) method. The SSR procedure is a direct geophysical-seismological approach that allows for the assessment of the potential amplification of a target site by the seismic ground motion. The method consists in determining the ratio of the Fourier spectrum from the ground motion at the target site, where some amplification is expected, to the spectrum of the ground motion at a reference site, free from any modification of the seismic signal (Borcherdt 1970). Unlike the HVSR (H/V) method, the SSR requires the use of a second seismic station installed on a hard rock (reference site), near the target site. The application of this method is also completed by other studies in some areas along the EPGF after the Haiti 2010 earthquake (St Fleur et al. 2016; Ulysse et al. 2018a, b, 2021).

The seismic events were recorded by four digital broadband seismometers CMG-6TD designed and manufactured by Guralp Systems Limited. The installations were carried out during the geophysical-seismological surveys at Anse-à-Veau (Nippes department) in January 2022. Two seismometers were installed at the study area, Anse-à-Veau for local amplification study, the other ones at Miragoane and Fonds des Nègres (two other municipalities in the Nippes department, see Fig. 2a) for seismological recordings in the Enriquillo Plantain Garden Fault Zone.

3.3 Seismic profiles

Seismic methods use the propagation of mechanical waves (body waves or surface waves) in the subsoil to determine the velocity distribution and thus locate the interfaces between different materials or layers. The seismic refraction tomography (SRT) provides a cross-section representing the different P-wave velocities of the soil layers below the line of the profile. The multichannel analysis of surface waves (MASW) provides a 1-D profile of S-waves velocities as a function of the depth.

SRT makes it possible to model the velocity distribution of the subsoil in 2D or 3D from the times of first arrival of the waves observed on the seismic recordings. The seismic velocities studied in tomography are mainly the velocities of the compression wave (P-waves) obtained by using the refraction properties of the wave at the interfaces between media with different properties. The P-wave arrives first at the sensors and is easily recognizable. The method involves creating an initial velocity model, for which the travel times are calculated along 'rays' and compared with the measured travel times; then, the model is iteratively modified in order to minimise the difference between the calculated and measured times. The essential objective is to find the minimum travel time between the source and the receiver for each source-receiver pair. Indeed, the maximum time might include slow or indirect paths while the minimum time is cleaner and more reliably associated with first-arrival energy.

MASW allows obtaining a 1-D model of shear waves (S-waves) as a function of depth using surface wave methods based on the inversion of the dispersion curve of surface waves (mainly Rayleigh waves)

assuming plane waves propagating in a horizontally stratified medium. The wave propagates in the ground at a speed which depends on the nature of the materials (their compactness). The method involves the calculation of a dispersion curve from seismic recordings and its inversion to find the 1D S-wave profile. The basic idea lies in the fact that in a heterogeneous medium, the phase velocity of Rayleigh waves is a function of the frequency and the mechanical characteristics of the medium. Thus, if the dispersion curve is measured, it is in principle possible to find the characteristics of the crossed medium by the inversion operation. From the 1D S-Wave profile, it is possible to deduce a standardized geomechanical parameter, V_{S30}, which is involved in soil classification according to the International Building Code or the Eurocode 8 (IBC or EC8). The V_{S30} is an average of the S-waves velocity over the first 30 m below the seismic profile on the site.

The SRT and MAWS surveys were carried out using a portable 24-channel seismograph, model DAQLink III, manufactured by the American company SEISMIC SOURCE. Equipped with a recording system 24-bit, the seismograph is controlled by computer, via an Ethernet cable, using driver software (VSCOPE™) provided by the manufacturer. A number of 24 receivers (geophones, generally with 5 m spacing) was used. The pulse source is produced by the impact, on a rigid plastic striking plate, of a 9.1 kg (20 lb) mass equipped with a seismic trigger compatible with the seismograph.

3.4 Electric profiles

The electrical method used is the electrical resistivity tomography (ERT), which allows obtaining an electrical image of the subsoil, e.g. a section of the resistivity as a function of depth by measuring the resistance profile for different combinations of electrodes and potential.

The first step in this method of investigation consists of carrying out a series of individual measurements using metal electrodes driven into the ground, generally along a profile (2D). These measurements are carried out according to a predefined sequence. The apparent resistivity values obtained for each of the measurement quadrupoles are reported in a vertical plane called pseudo-section. In order to calculate the true or interpreted resistivity of the subsoil at each point of the vertical section, the apparent resistivity values must be inverted (Reynolds 1997). Mathematically, the objective of the inversion is to minimize the difference (which is expressed by the RMS function: Root Mean Square) between the values of the calculated pseudo-section for the soil model and those of the measured pseudo-section. The soil model obtained at the end of the inversion constitutes a solution, which is not unique regarding the values of the true or interpreted resistivities of the subsoil (Oldenburg and Li 1994). To stabilize the solution and reduce the non-uniqueness, a regularized inversion is used by applying the L-curve method.

Depending on the different configurations, the current is injected via two injection electrodes and the potential difference is measured between two other (measuring) electrodes. Among the configurations (Wenner, Schlumberger, Dipole–dipole, etc.) conventionally used, the Wenner configuration is more sensitive to a vertical variation in resistivity, whereas the dipole–dipole configuration is influenced by a horizontal variation in resistivity.

The equipment used to perform the ERT measurements is the Terrameter SAS system from ABEM. It consists of a basic unit called Terrameter SAS 1000/4000 which can be supplemented as desired with accessories such as the ABEM LUND electrode systems and the ABEM SAS LOG borehole logging unit. The Wenner configuration was mostly used during these surveys.

3.5 Geostatistical analysis and geomodelling

Geostatistics were initially developed to analyse geological data in the mining sector (Matheron 1970; Armstrong and Carignan 1997) but can be applied to any natural phenomenon that presents a spatial distribution according to a certain structure (Chauvet 1999). As introduced above, the geostatistical technique is now widely applied in geosciences to assess spatial relationships between collected data, including those produced by geophysical prospecting (Bourges et al. 2012).

The geostatistical analysis is based on the variogram $\gamma(h)$ which is a function that summarizes the essential structural features of the studied phenomenon and defines the dissimilarity between two experimental data at locations separated by a vector h (Armstrong and Carignan 1997; Bourges et al.

2012). The final process can be done by kriging or geostatistical simulation. Kriging is the unbiased linear estimator that ensures minimum estimation variance (Myers 1989; Chauvet, 1999), but simulation methods are necessary when we want to obtain a spatial model that has the same variability characteristics as the real phenomenon. Appropriate methods are developed in nonlinear geostatistics but, unlike the simulation methods, they do not allow estimation when the criteria are complicated, nor to quantify the confidence in the estimators.

The cokriging, a multivariable generalisation of the kriging, is applied to the H/V and MASW results following the coregionalization linear model which describes not only the spatial organisation of each of the variables but also their joint organization. The superiority of cokriging over kriging in minimizing estimation variance is amply demonstrated when the secondary variables are highly correlated with primary variables (Wu et al. 2009; Emery 2012).

Conditional simulation is used to classify the sites according to their potential lithological sites effect and to establish the geomodel. It is a method commonly used to generate multiple realizations of spatial fields, which are consistent with observed data and satisfy known constraints, such as geological boundaries or other geosciences data (Journel and Huijbregts 1978; Isaaks and Srivastava 1989). The conditional simulation provides a means to understand the variability of spatial processes by accounting for both the spatial continuity of the variable and the local conditions at the sampling points (Chilès and Delfiner 2012; Cressie 2015). The simulation applied to our data is conditional in the sense that the models simulated are constrained by the H/V data and the profiles. First, the relationship between the H/V and MASW data is used to compute the depth of the shallow layers, then the depth is conditionally simulated to establish the contact surface between the layers and construct the geomodel.

The present study remains within the framework of the two-point geostatistics method. Indeed, the variogram tool used here define the dissimilarity between two points, by opposite to new method called multipoint statistics (MPS) technique (Mirowski et al. 2008; Avalos and Ortiz 2020). However, the latter uses a structural tool called training image (the equivalent of the variogram in the MPS) which is too subjective and not developed enough in the available software for practical application.

3.6 Local ground motion assessment

The spatial methods for local ground motion assessment offer a complementary approach to the more conventional numerical modelling studies, which often require significant computational resources and assumptions about input parameters. They allow for the integration of the regional seismic hazard with high-resolution spatial data to estimate the varying ground motion at local scales (Joyner and Boore 1993; Atkinson and Boore 2003). These methods involve the mapping of the site using geomorphological investigation and geophysical surveys which can then be coupled with empirical models of site amplification (Borcherdt 1994).

The current seismic hazard maps for Haiti by Frankel et al. (2011) had been established by using the probabilistic method and the next generation attenuation (NGA) laws (Boore and Atkinson 2008; Campbell and Bozorgnia 2008; Chiou and Youngs 2008) for the crustal faults. Besides the magnitude and distance terms, these attenuation laws include a site amplification term via the parameter V_{s30}. Frankel et al. (2011) calculated the magnitude and distance terms for each NGA separately, but they used the site amplification formula from Boore and Atkinson (2008) NGA for all of them. The latter is a function of V_{s30}, period, and the calculated Peak Ground Acceleration (PGA) for a rock site.

The present study uses an updated version of Boore and Atkinson (2008) NGA relations for the assessment of the local ground motion. For the site amplification formula, the updated version from Boore et al. (2014) includes a depth term besides the V_{s30}. The V_{s30} map from the MASW results and cokriging technique using the fundamental frequency f_0 as secondary variable are expected to be used in the site amplification formula of Boore et al. (2014) to assess the local ground motion.

4 Results

The surveys carried out for the present study include more than 150 H/V measurements, 8 ERT profiles, 22 SRT-MASW profiles and the earthquake recordings

from two broadband seismometers at Anse-à-Veau, and two other ones at Miragoane and Fond des Nègres, near the EPGF.

4.1 HVSR results

The H/V data (~150) consist of ambient noise recordings of 20 to 30 min with a rate of 128 samples per second processed by the Geopsy software (Wathelet et al. 2020). The time windows used have a length between 20 and 40 s and can overlap by 5%. The anti-triggering algorithm to avoid the transient noises is based on the comparison between the short term (STA) and long term (LTA) average amplitudes. The values for STA, LTA, minimum STA/LTA and maximum STA/LTA are 2, 30, 0.2 and 2.5 s, respectively. The smoothing function of Konno & Ohmachi are applied with a bandwidth coefficient *b* of 40 and a cosine taper of 5%. The analysis is made in the frequency range 0.25–25 Hz.

The measurements were performed in town area, near the sea and other isolated area. The final results are the H/V curves as a function of the frequency of the site and its relative amplitude. The shape of the H/V curves and their frequency indicate the potential of the site to locally amplify seismic ground motion. Figure 3 shows the location and the fundamental frequency obtained within the area with indication of some H/V curves characteristics.

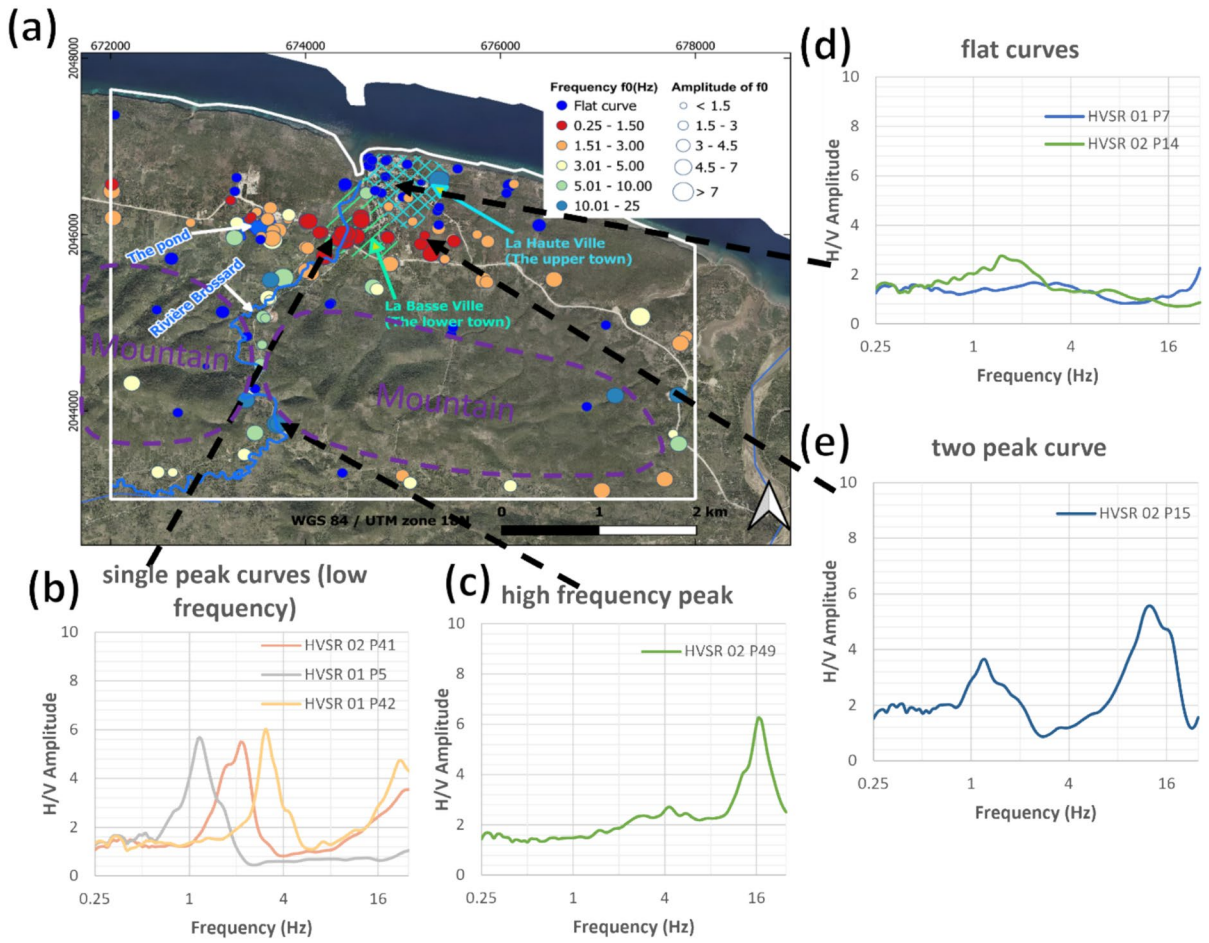

Fig. 3 (**a**) Some characteristic HVSR results obtained from the ambient noise measurements. Color of circle on the map indicates the fundamental resonance frequency f_0; size of circle indicates the relative amplitude of the f_0 peak. (**b**) single peak H/V curves at low frequency in *La Basse Ville*. (**c**) single peak curve at high frequency in southwest of the study area. (**d**) flat curves in *La Haute Ville*. (**e**) H/V curves with two peaks in the area of marly limestone covered by laterite soil

The flat curves are localized at *La Haute Ville* on the Quaternary reef limestone. The curves become less flat, but with a weak amplitude, in the south of *La Haute Ville* in the contact zone between the Quaternary reef limestone (of *La Haute Ville*) and the pelagic massive limestone of the mountain. This contact zone (mainly characterized by marly limestone) is covered in some parts by laterite soils where the H/V curves show two peaks, the first of which may correspond to the marly limestone and the second, at higher frequency and amplitude, may correspond to the superficial deposit of the laterite soils.

The low frequencies and high amplitudes in *La Basse Ville* indicate a clear site amplification potential. Some peaks with the higher amplitudes are also observed near the municipality of Arnaud (southwestern corner of the map), but they typically appear at higher frequencies. The low frequency with low-amplitude peaks in *La Haute Ville* indicate a lower site effect potential.

The azimuth analysis according to the H/V processing and the variographic analysis with anisotropy are shown in the Fig. 4; they indicate the same preferential direction for the wave propagation and the spatial variability of the shallow layer. The general direction following by the azimuth analysis of the ambient noise from Geopsy (Fig. 4a) shows that the shallow layer has been deposited following a trend roughly parallel to the direction of the mountain (~N110°). The shallow layer becomes thicker at *La Basse Ville* and towards the pond according to the peak at lower frequency but with Quaternary alluvium. The polarisation is orthogonal to the mountain near the coast at *La Basse Ville* (the direction of the river seems to influence the alluvium deposit near the coast), but it is roughly parallel to the direction of the mountain in the contact zone between the Quaternary reef limestone and the pelagic massive limestone of the mountain (the direction of the mountain seems to influence the sedimentary deposit in this contact zone).

The anisotropy from the geostatistical analysis (applied to the fundamental resonance frequency f_0) is visualized trough the variogram map (Fig. 4b) and indicate a more continuous behaviour of the fundamental frequency in a direction close to that of the azimuth analysis from Geopsy. The omnidirectional variogram (Fig. 4c) shows nugget effects, which are not removed to ensure the stability of the Gaussian model. These effects either correspond to error measurements or to microscale structures.

The theoretical Gaussian variogram is used to model the experimental variogram (Fig. 4c). It represents the spatial variability of the fundamental frequency, then the spatial behaviour of the potential site effects within the study area. The classical variogram models such as the spherical and exponential models have not been used since they correspond to continuous but not differentiable variables. They represent phenomenon with spatial autocorrelation that decreases rapidly even for small distances (Armstrong and Carignan 1997).

4.2 MASW results

The MASW method was mostly performed on profile of 115 m (24 geophones, 5 m spacing) and processed using the software SeisImager, Geometrics. The procedure consists of computing a dispersion curve from the input data and creating initial S-waves velocity models by considering various layers number and thickness. The final *Vs* model is an inverted model obtained by iteratively minimizing the RMS (Root Mean Square) between the observed and the theoretical data. The parameter V_{S30} is also deduced for every *Vs* profile.

The results obtained for some of the sites at Anse-à-Veau are presented in Fig. 5. The models obtained for *La Basse Ville* are combination of two dispersion curves. One is from the common active MASW method described above; the other one is from passive MASW technique using ambient noise. Indeed, the energy generated by the shots in the active method, differently from the energy from ambient seismic noise, could not reach the deeper parts of the very soft layers at *La Basse Ville*. The combined dispersion curves are slightly smoothed while merging the two individual curves (from active and passive sources). Then, the contrasts are not clear in the *Vs* profiles for *La Basse Ville* despite that we observed clear peak in the HVSR curves.

The *Vs* values are higher (> 600 m/s) at *La Haute Ville* on the Quaternary reef limestone and lower (100–250 m/s) at *La Basse Ville* on the Quaternary alluvium. The sites located between *La Haute Ville* and the mountain, and on the other side of the mountain in the southern part of the study area, are characterized by intermediate *Vs* values (400–450 m/s).

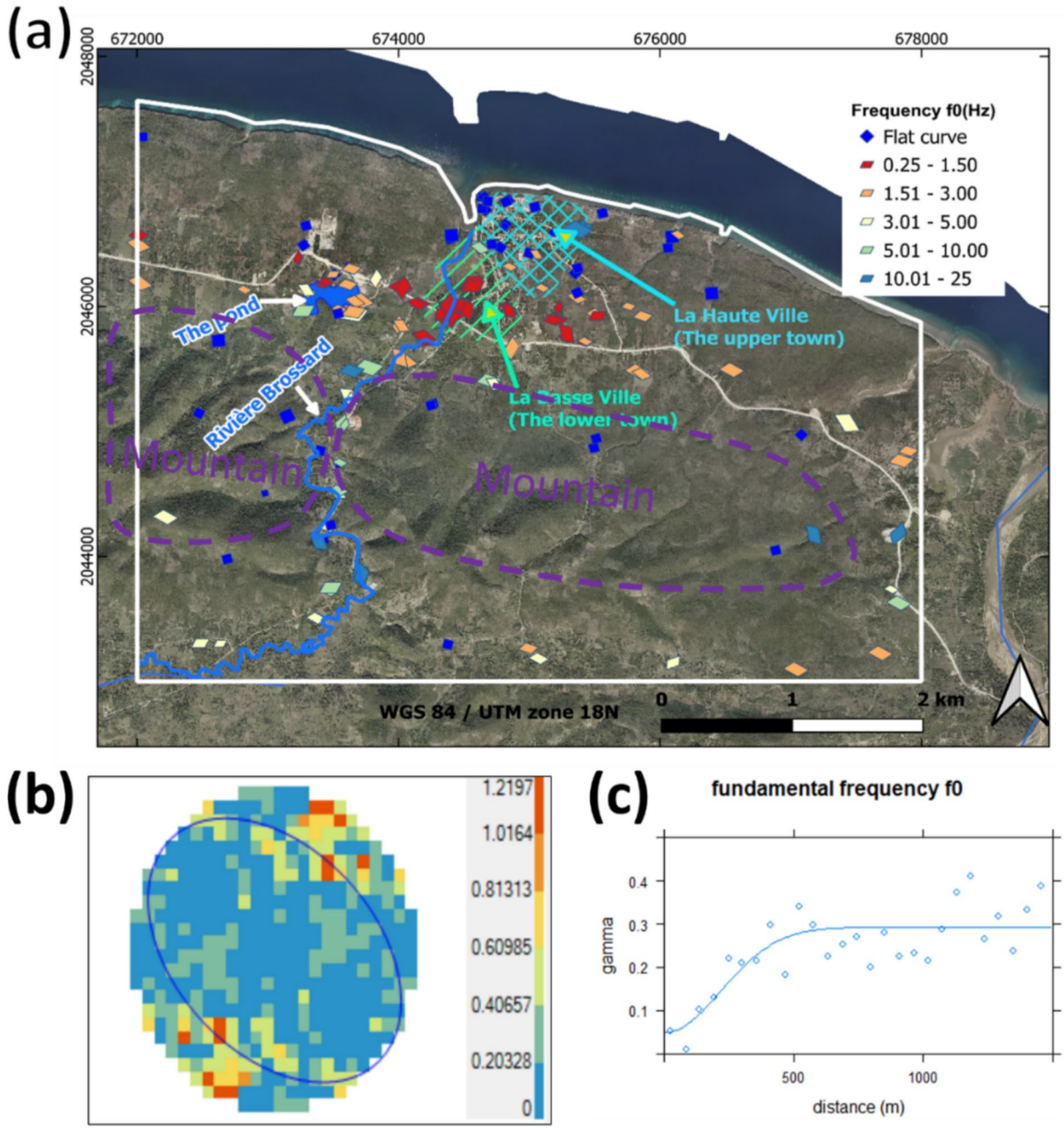

Fig. 4 (**a**) Azimuth analysis of the ambient noise HVSR measurements. The orientation of the diamonds long diagonals represents the direction of the wave polarisation. (**b**) and (**c**) the variogram map and model for the log distribution of fundamental frequency

They correspond to the sites with intermediate H/V curves between clear peak and flat H/V curves.

The MASW results are combined with the H/V results to produce a map of the parameter V_{S30} following the geostatistical analysis. The amount of the H/V data allows to take advantage of the cokriging technique and give more coherence to the final V_{S30} map since the H/V and the MASW results are highly correlated. The map is constructed with the gstat R package (Gräler et al. 2016) in the QGIS environment and presented in Fig. 6. The simple variograms (for each dataset) and cross-variogram (between the H/V

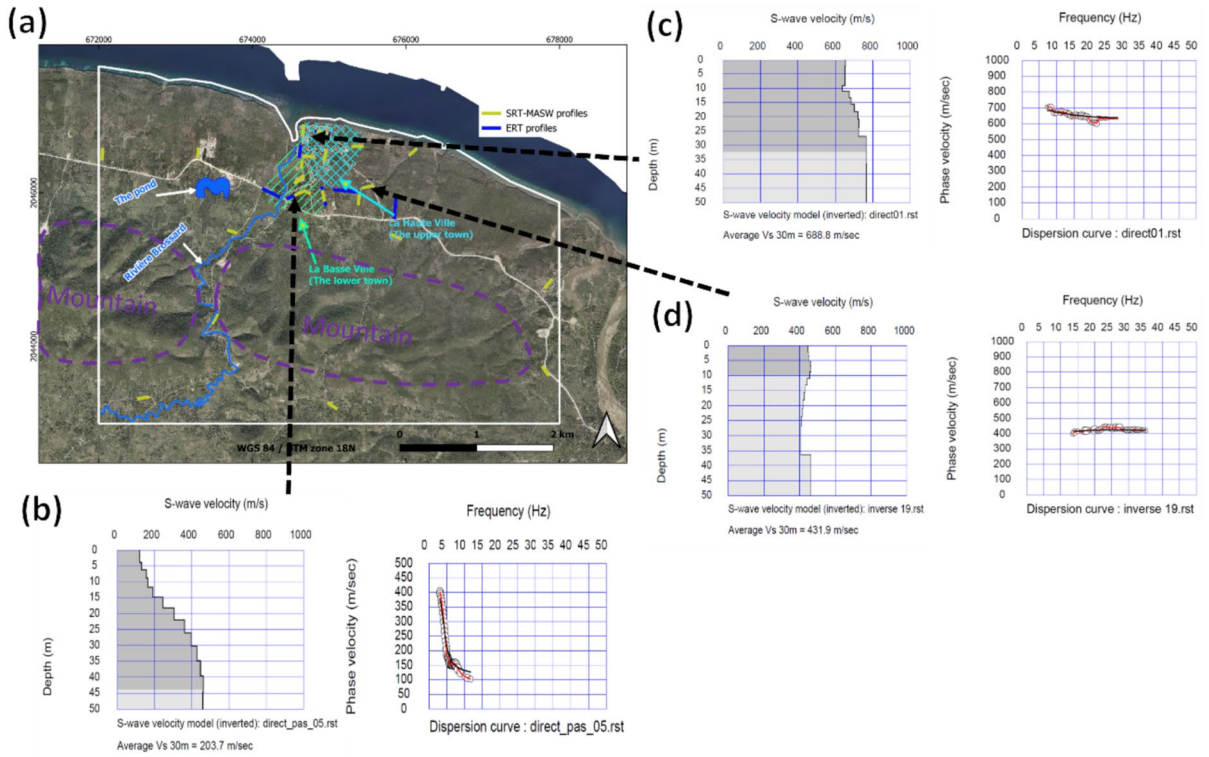

Fig. 5 (**a**) Seismic profiles carried out in Anse-à-Veau. (**b**) S-waves velocity profile (*Vs*) and dispersion curve for a site in *La Basse Ville*. The grey areas in the profiles are computed from the data; the lower areas are interpolated by the processing software to represent the deeper parts. The red curves represent the experimental dispersion curves; the black ones are the theoretical curves from the inversion process. (**c**) S-waves velocity profile (*Vs*) and dispersion curve for a site in *La Haute Ville*. (**d**) S-waves velocity profile (*Vs*) and dispersion curve for a site in the contact zone between the Quaternary reef limestone (of *La Haute Ville*) and the pelagic massive limestone of the mountain

and MASW data) were modelled together, since there are mathematical restrictions between them (Emery 2012). The linear model of co-regionalisation used assumes that simple and cross-variograms are linear combinations of the same theoretical basic models. The V_{S30} map is a first attempt to construct a potential site effects index map for the local ground motion assessment.

4.3 SRT and ERT results

The SRT profiles, carried out with the same configuration as the MASW, were also processed with the software SeisImager, Geometrics. The input data were analysed by picking the first arrivals (P-waves) for every signal and computing the travel time curves. Like in the MASW procedure, the final P-waves velocity (*Vp*) model is obtained by minimizing the RMS between the theoretical and the observed travel times.

The ERT profiles were processed with the RES-2DINV software (Loke and Barker 1996) using a generalized least squares optimisation method to automatically determine a (2D) subsurface resistivity model for the input data. The pseudo-section obtained with the input data is divided into several rectangular blocks (with an apparent resistivity value for each block) whose size increases with depth. Iteratively, RES2DINV attempts to minimize the difference between the calculated and measured apparent resistivity values.

The results obtained for some of the sites at Anse-à-Veau are presented in Fig. 7. The *Vp* values vary from 300 m/s for the superficial soft layer to 3000 m/s for the hard rock. The resistivity values vary from 0.1 to 3000 Ω.m across the ERT profiles. They are generally low

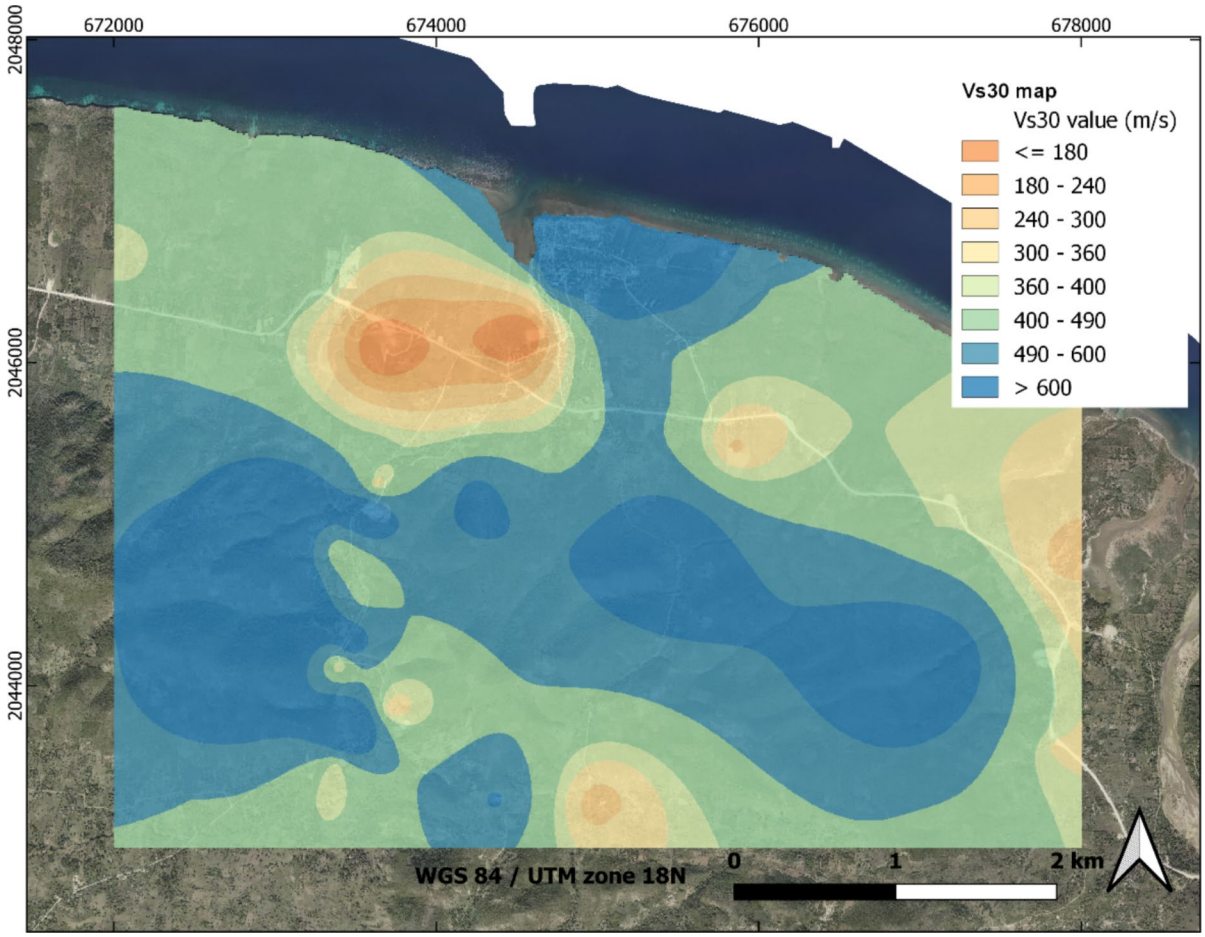

Fig. 6 V_{S30} map obtained by applying the cokriging technique between the MASW and the H/V results

for the soft and fine soils and high for the granular soils and hard rock. However, the presence of saturated and salted materials tends to modify the resistivity of the soil like in the resistivity section in Fig. 7c. The presence of the small portion of high resistivity at the bottom of the cited profile could be explained by the infiltration of the sea in the layer.

The results of the SRT and the ERT profiles show that the layers with low resistivity and low *Vp* are located in *La Basse Ville* on the Quaternary alluvium, in the contact zone between La Haute Ville and the mountain and in the eastern part of the study area.

4.4 SSR results

4.4.1 The reference seismic station

As stated in the methodology, the application of the SSR technique requires at least one reference station installed on a site with characteristics of a bedrock, and one or more other stations installed on the target site where some amplifications are expected. The geophysical characteristics of the reference site are presented in Fig. 8. The reference site is located in the *La Haute Ville* part on the high reef limestone

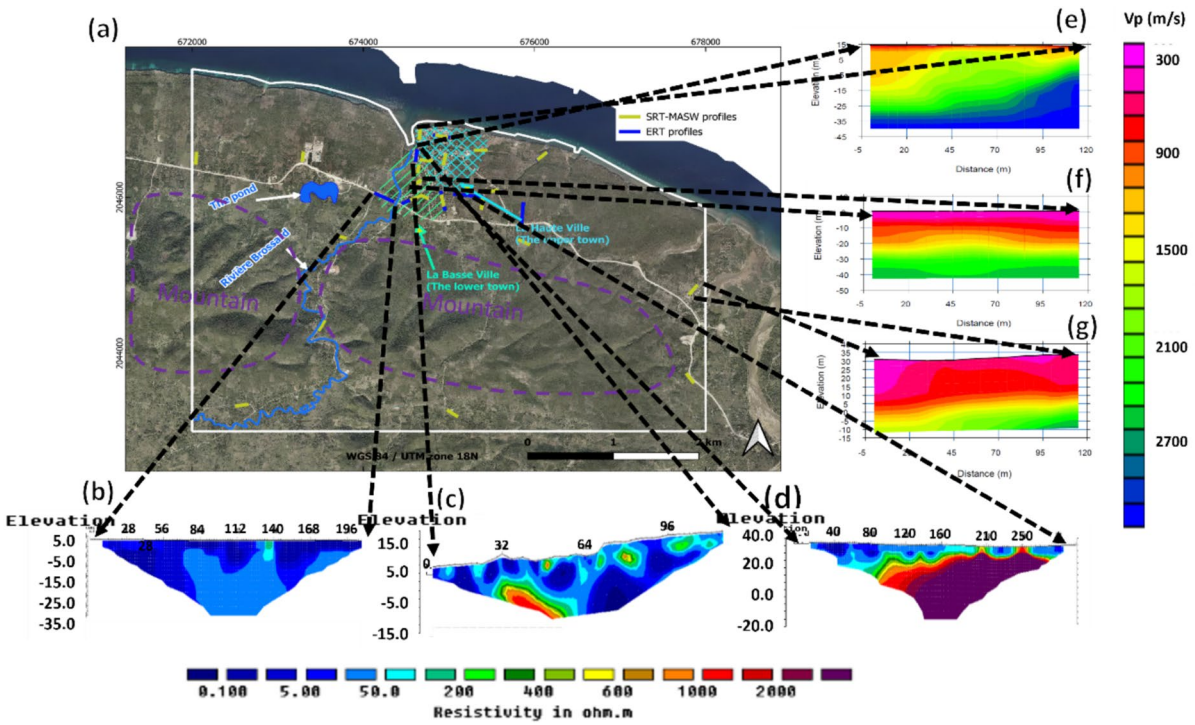

Fig. 7 ERT (**b-d**) and SRT (**e–g**) profiles obtained for some of the sites at Anse-à-Veau. The colour scale is different for seismic and electrical cross section, but the same within each profiles type (ERT and SRT separately)

(Fig. 8a). The H/V curves (Fig. 8b and c) are flat with very low amplification. The MASW profile (Fig. 8d) shows values of *Vs* below 760 m/s in the first 5 m that increase with depth. The SRT profile (Fig. 8e) shows *Vp* values that rapidly increase below 5 m of depth (> 1000 m/s).

The seismic station at the reference site in *La Haute Ville* (the upper town of Anse-à-Veau), the one at the target site in *La Basse Ville* (the lower town) as well as the two others in Miragoane and Fonds des Negres along the EPGF (see Fig. 2) recorded any vibrations including real seismic event and ambient noise. The location and the magnitude of the recorded earthquakes have not been computed in this study, but directly collected from the platform Ayiti Séismes (https://ayiti.unice.fr/ayiti-seismes/) and the Technical Unit of Seismology (UTS-BME, Haiti). Indeed, for the earthquake EQ 005 presented in Fig. 9a, the seismogram is from the reference station (UR02), but the location and the magnitude are collected from the mentioned platform by using the exact recording date and time to retrieve the same event. The time displayed in the seismogram is UTC time. The H/V curves for this earthquake (HVEQ) and the ambient noise (HVSR) recorded by reference station are presented in Fig. 9b and c. Both H/V curves are relatively flat with low amplitude and correspond to a site with no local amplification in the input seismic waves.

4.4.2 The SSR in the target site

The SSR method is performed on the earthquakes presented in Table 1 and Fig. 10. The seismic station used as target is located in *La Basse Ville* (inside the black ellipse, Fig. 11a) where local amplification always occurred according to observations from recent earthquakes (like the 2021 Nippes earthquake) and historical seismicity reports. For a selected earthquake, the Fourier spectrum of each horizontal component from this target seismic station is divided respectively by the corresponding one from the reference station. The SSR is applied for the tail of seismic waves where the part of the signal is not saturated. The earthquakes are separated into three groups based on their location with respect to the target

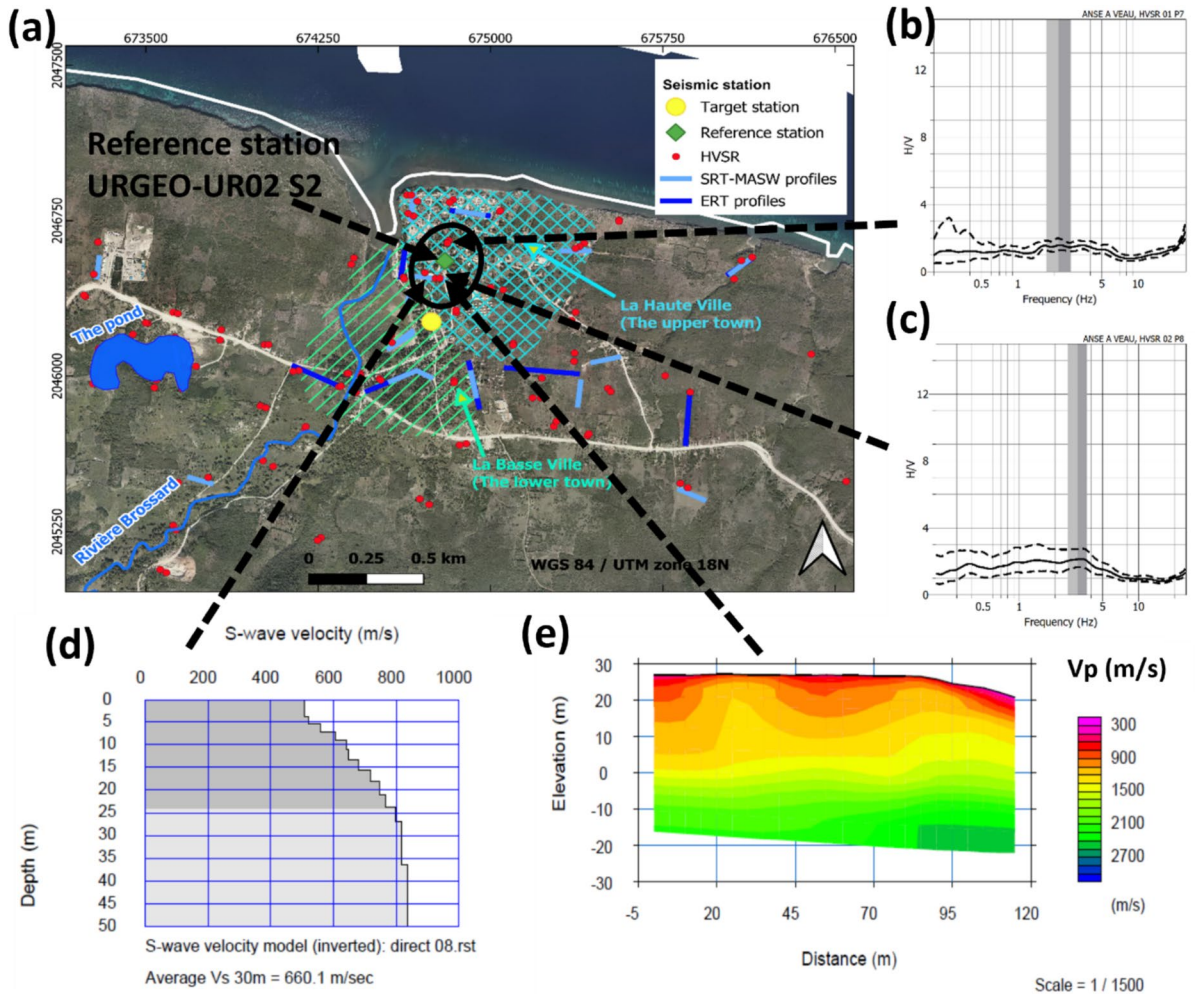

Fig. 8 (**a**) Location of the reference station UR02 S2 in *La Haute Ville* on the reef limestone. (**b**) and (**c**) Flat H/V curves obtained from ambient noise recorded at the site by the Tromino (Sect. 3.1). The dashed black lines represent the standard deviation estimated for H/V curves calculated from 20 to 30 individual time windows. (**d**) Seismic profile *Vs* from MASW method. (**e**) SRT profile (P-wave velocities)

station: GNE in the north-east, GE in the east and GSE in the south-east (Fig. 10). The results presented in Fig. 11b-c and Fig. 12 include the SSR curves for one of the earthquakes (EQ006), for each group, and the average SSR curves for all the selected earthqua kes.

The SSR curves for the single earthquake EQ006 (Fig. 11b-c) show two different peaks at the frequencies of ~ 2 Hz and ~ 6 Hz on the E-W component (Fig. 11b). However, the peak at ~ 2 Hz is less clear on the E-W component for the SSR curves (Fig. 12a, c and e) computed for all the distinct groups of earthquakes (GNE, GE and GSE; see Fig. 10). On the E-W component of the averaged SSR curves (Fig. 12g), a peak at ~ 3 Hz is observed (while it appears less clearly on the SSR curves of the respective earthquakes' groups, or on the single SSR curve of EQ006, see Fig. 11b). The peaks at frequencies of ~ 3 Hz and ~ 6 Hz are also observed on the N-S component for the average SSR curve (Fig. 12h), the respective earthquake groups (Fig. 12b, d and f) and the single EQ006 event (Fig. 11c). The H/V curve obtained for the selected earthquake (EQ006) is characterized by weakly pronounced peaks at approximately 2 Hz and 3 Hz.

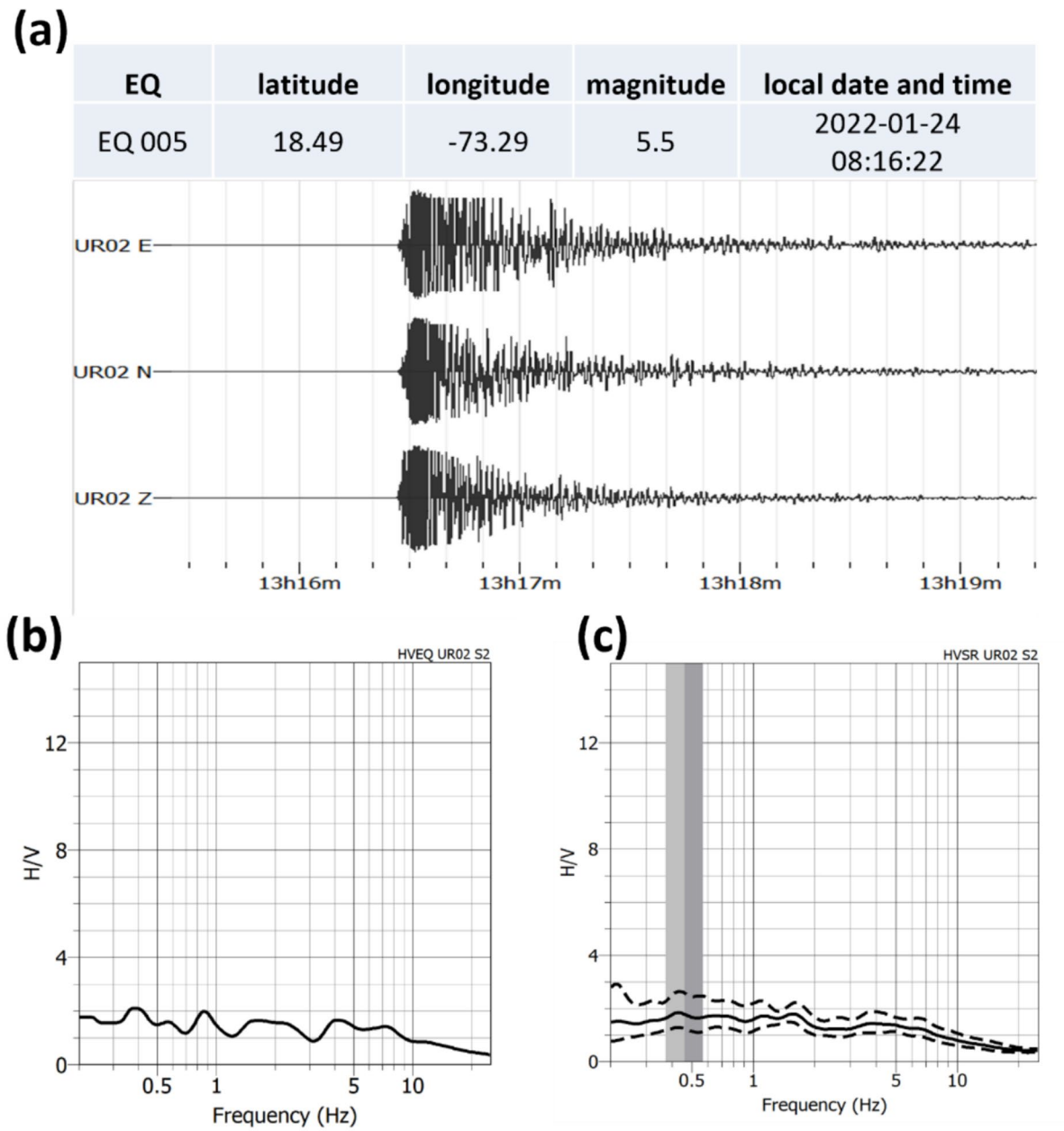

Fig. 9 (**a**) Earthquake recorded by the reference station UR02 S2. (**b**) H/V of the earthquake recorded by the reference station. **(c)** H/V of ambient noise recorded by the reference station. The dashed black lines represent the standard deviation estimated for H/V curves calculated from 20 to 30 individual time windows

The lithology at the target station seems to be complex as the site is located near the edge of the alluvium deposit. The peak observed at ~ 6 Hz in the two components (E-W and N-S) for all the SSR curves (single, group and total average) may be due to a very simple superficial deposit. For the peaks at lower frequency (2 Hz and 3 Hz), the presence of the first one in only the E-W component (and the second one in the N-S component) may correspond to a complex underlaying layer in the edge of the alluvium deposit.

Table 1 Summary of the earthquakes (EQ) selected for the application of the SSR method

EQ	latitude	longitude	depth (km)	Magnitude (Mw)	local date and time
EQ 005	18.54	−73.29	2.5	5.5	2022–01-24 08:16:22
EQ 006	18.49	−73.29	8.5	3.7	2022–01-24 08:21:26
EQ 007	18.55	−73.31	4.5	4.6	2022–01-24 08:43:16
EQ 008	18.55	−73.3	1.5	5.4	2022–01-24 09:06:41
EQ 010	18.54	−73.29	3.5	4.2	2022–01-24 09:14:30
EQ 011	18.49	−73.27	6	4.3	2022–01-24 10:08:30
EQ 012	18.45	−73.25	7	3.6	2022–01-24 13:32:23
EQ 015	18.48	−73.29	10	4.5	2022–01-24 15:01:45
EQ 018	18.42	−73.19	7	4.3	2022–01-24 18:26:46
EQ 020	18.45	−73.24	10	4.2	2022–01-24 21:27:29
EQ 021	18.44	−73.26	11	4	2022–01-25 01:06:05
EQ 023	18.48	−73.25	8.5	3.7	2022–01-25 11:51:33
EQ 024	18.56	−73.33	17.5	4.6	2022–01-25 13:50:57
EQ 025	18.53	−73.34	3	4.6	2022–01-25 20:14:28
EQ 031	18.44	−73.27	11.5	3.9	2022–01-26 13:05:22
EQ 035	18.55	−73.25	4.5	4.3	2022–01-28 16:50:26
EQ 039	18.44	−73.28	13	4.3	2022–01-30 04:22:29
EQ 046	18.48	−73.49	7	4.3	2022–05-02 10:41:16
EQ 047	18.47	−73.31	7	3.6	2022–05-06 22:13:06
EQ 048	18.39	−73.45	9	3.6	2022–05-08 19:27:12
EQ 049	18.48	−73.58	9	4.4	2022–05-09 12:45:53

The higher amplitudes related to the 3 Hz peak in the N-S components could be explained by the polarisation of the wave in a N-S direction as suggested by the azimuth analysis for some of the ambient noise H/V near the target site (see Fig. 4). Indeed, the earthquakes directional effect does not really affect the difference of amplitude (observed in E-W and N-S component) according to the SSR results of the three selected group.

4.5 The geomodelling results

The geomodelling is carried out with the software Leapfrog Works (Sequent Limited). The H/V measurements coupled with the MASW profiles are represented as boreholes with a depth according to the surface layer thickness computed as follows. The cokriging method (from geostatistics) allow taking advantage of two spatially correlated data (even though they are not the same type). Since we have more sites with H/V data than MASW, we used the cokriging method to estimate the MASW data (S-waves velocity, *Vs*) in the sites where we only had H/V data (fundamental frequency, f_0). First, we obtained a couple of fundamental frequency (f_0) and S-waves velocity (*Vs*) values for every H/V location; second, the formula $h = Vs/(4 \times f_0)$ is used to calculate the depth h of the sedimentary deposits in these locations (see Sect. 3.1). The contact surface between the layers within the geomodel is the depth h simulated by geostatistical methods using a fine grid in the R/RStudio environment. The simulation was conditional since the H/V and MASW original data as well as the SRT and ERT profiles have been used as constraints. The geomodel is presented in Fig. 13 with a roughly E-W trending cross section obtained from the 3D model.

The formations in the geomodel (Fig. 13) are based on the interpretation of the geophysical data as well as the geomorphological context of the study area. The alluvium formations are characterized by clear peak H/V curves at low frequency with high level of lithological amplification and low *Vs* and *Vp* values. The formations identified as marly limestone are mainly both in a contact zone between the reef limestone of *La Haute Ville* and the pelagic massive

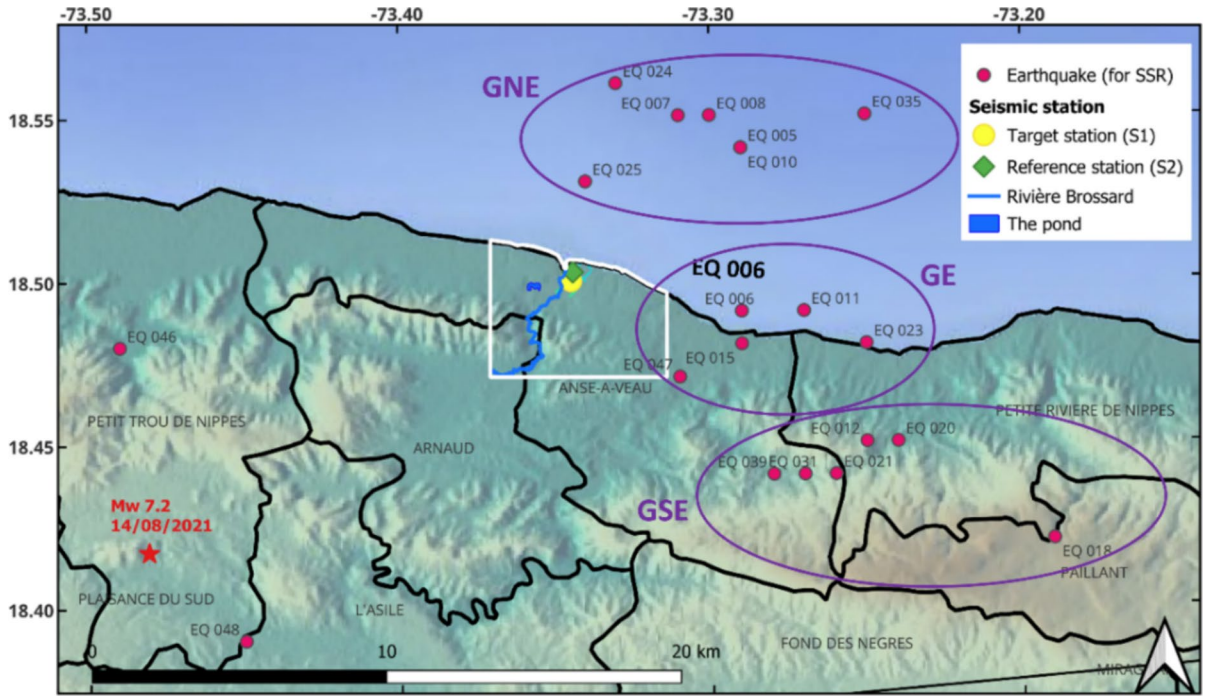

Fig. 10 Locations of the earthquakes (EQ) selected for the application of the SSR method. They are separated into three groups based on their location with respect to the target station: GNE in the north-east, GE in the east and GSE in the south-east. The study area is delimited by the white polygon. The distance between the target station (S1, the yellow circle) and the reference station (S2, the green diamond) is very small with respect to the distance to the earthquakes epicentre. The red star indicated the location of the 14 August 2021 earthquake

limestone of the mountain, and at south of the mountain. They are characterized by one or two peaks H/V curves with intermediate level of lithological amplification; in the southwest part, the peak is observed at high frequency due to the presence of superficial marly limestones with high clay content in the vicinity of the river. The laterite formation is a small area of red soil within the marly limestone where the H/V curves show two peaks. The basement is a set of formations that include the area in La Haute Ville characterized by the high reef limestone and flat H/V curves with no lithological amplification, the massive pelagic limestone of the mountain, and the bedrock beneath the shallow deposits.

4.6 The local ground motion

The ground motion assessment is based on two sets of attenuation relationship that compute the Peak Ground Acceleration (PGA) for the southern peninsula with no site effects and for the study area with the site effects. The first attenuation equation is from Boore and Atkinson (2008) of the Next Generation Attenuation (NGA) and was used in the seismic hazard maps for Haiti by Frankel et al. (2011). The second equation is from Boore et al. (2014) and can be seen as an update version of the first one.

The results presented in Fig. 14 are the potential PGA generated by the 14 August 2021 earthquake for a uniform firm rock site with a V_{S30} of 760 m/s across the southern peninsula. In Fig. 15, we present a map of PGA estimated from ground shaking with data compiled by US Geological Survey (https://earthquake.usgs.gov/earthquakes/eventpage/us6000f65h/shakemap/analysis).

The maps computed from the NGA (Fig. 14) show high PGA values (> 0.5 g) concentrated along the fault segment involved in the M 7.2 Nippes 2021 earthquake that are rapidly attenuated with the distance. The estimated PGA map (Fig. 15) from ground shaking show high values (> 0.5 g) around

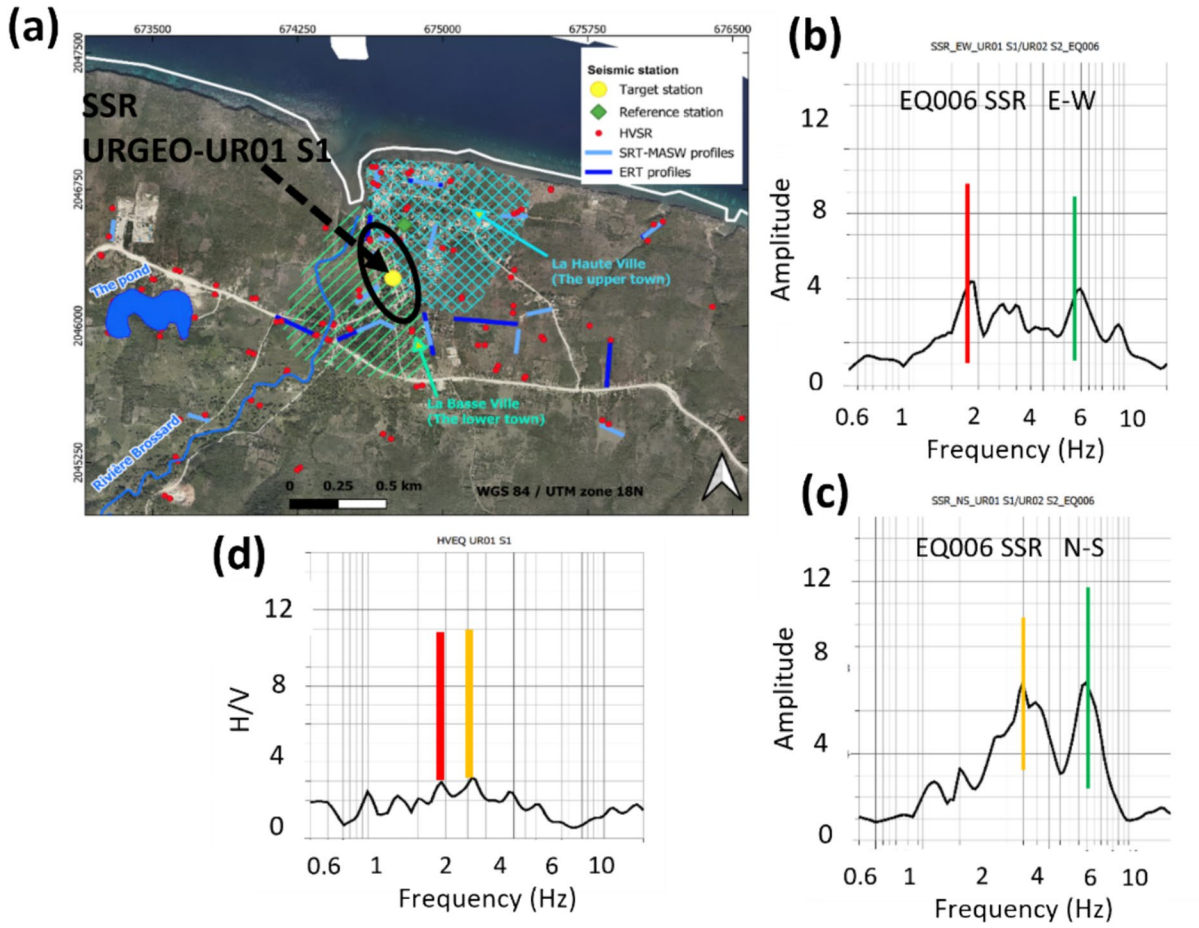

Fig. 11 (**a**) Location of the target station UR01 S1 in La Basse Ville on the Quaternary alluvium. (**b**) SSR in the E-W direction for the earthquake EQ006 (see Fig. 10) at the target station UR01 S1 with respect to the reference station UR02 S2 for two of the recorded earthquakes. (**c**) SSR for the same event in the N-S direction. (**d**) H/V curves from an earthquake recorded by the target station

the epicentre (and the other end of the segment fault) that are more gently attenuated with distance.

For the study area, we use the NGA from Boore et al. (2014) to calculate the site amplification term with the V_{S30} from the MASW. The maps presented in Fig. 16 are constructed by considering the linear site amplification term (Fig. 16a) and both (linear and nonlinear) site amplification (Fig. 16b). The value of the PGA is higher in the area with low V_{S30} value when considering only the linear site amplification term. When including the non-linear term, the PGA still increases when V_{S30} value decreases; however, below 360 m/s, the inverse phenomenon is observed. The latter could correspond to attenuation related to non-linearity behaviour of the soft layers below 360 m/s.

5 Discussion and conclusion

The area of Anse-à-Veau is marked by the presence of a series of lithological and morphological features that can increase the local ground motion during an earthquake. Instrumental and historical seismicity (Scherer 1912; Flores et al. 2012) confirm the high level of seismic activity in the region and the damage distribution inside the area. The reports of the damage caused by the 14 August 2021

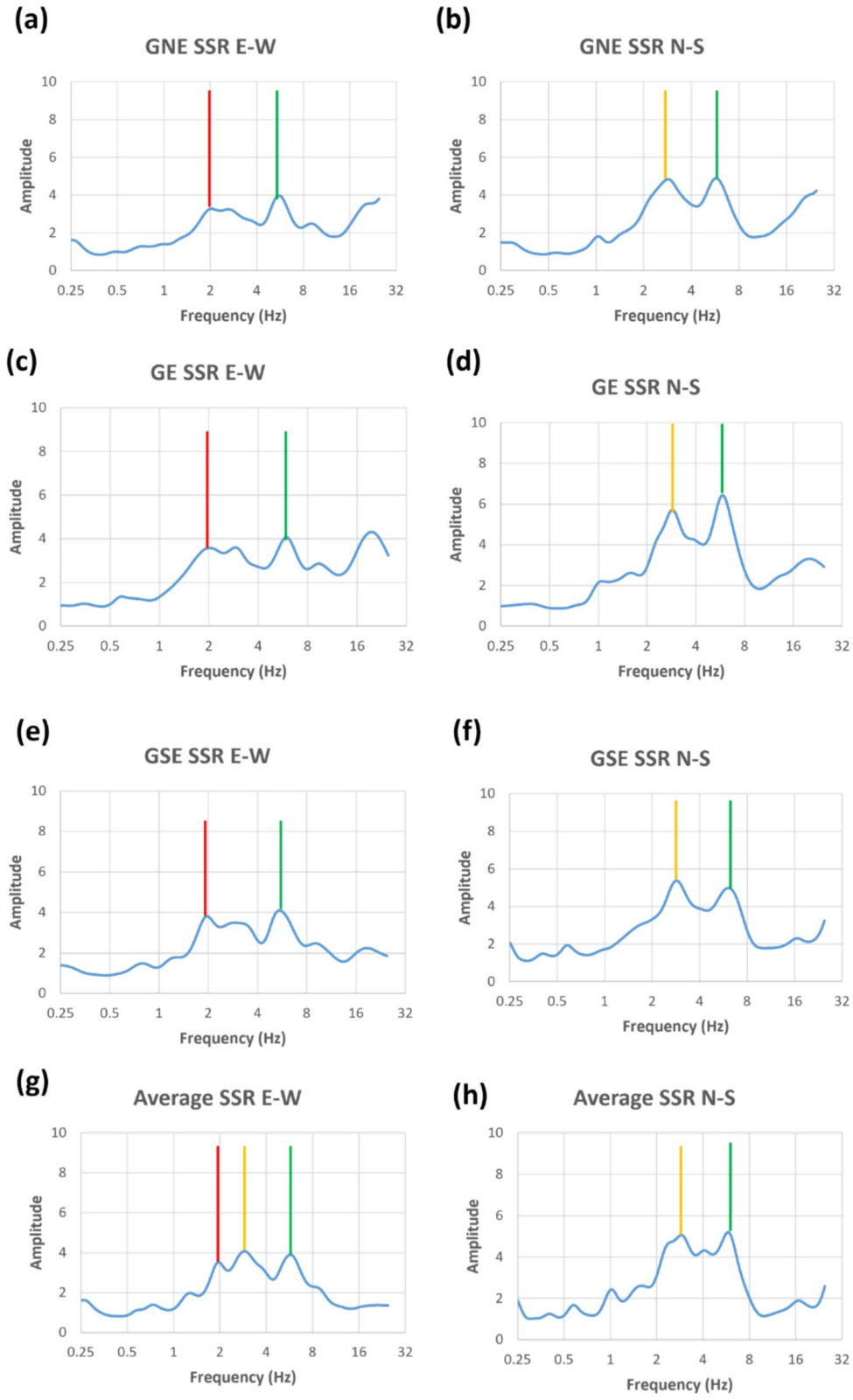
(a)
GNE SSR E-W
(b)
GNE SSR N-S
(c)
GE SSR E-W
(d)
GE SSR N-S
(e)
GSE SSR E-W
(f)
GSE SSR N-S
(g)
Average SSR E-W
(h)
Average SSR N-S
Amplitude
Frequency (Hz)
0.25
0.5
1
2
4
8
16
32
0
2
4
6
8
10

◂**Fig. 12** Results of the SSR method applied at the target station UR01 S1 with respect to the reference station UR02 S2 for the selected earthquakes in Table 1 and Fig. 10. (**a**) and (**b**) SSR curves in E-W and N-S components for the earthquakes in the group GNE (see Fig. 10). (**c**) and (**d**) SSR curves in E-W and N-S components for the earthquakes in the group GE. (**e**) and (**f**) SSR curves in E-W and N-S components for the earthquakes in the group GSE. (**g**) and (**h**) SSR curves in E-W and N-S components for all the earthquakes

earthquake, highlight the presence of local amplification in the area of Anse-à-Veau and are in good agreement with geomorphological and geophysical structure of the study area.

The present local amplification assessment is mainly experimental with geostatistical simulation of the main parameters. It confirms, like a series of previous studies (Ulysse et al. 2018a, b; Hakimov et al. 2021), that the H/V method combined with other geophysical-seismological data can strongly support site effect analysis in areas covered by soft sedimentary deposits. The fundamental frequency obtained from the H/V curves coupled with the *Vs* from MASW profiles allow defining a depth parameter. The joint analysis of these two results shows that low *Vs* values correspond to the sites with clear peak H/V curves and are mainly located in the Quaternary alluvium deposit as expected.

The sites with lower fundamental frequency and higher relative amplitude are located in *La Basse Ville* and near the pond. The fundamental frequencies increase when we move away from these areas. The opposite phenomenon is observed for the amplitudes. The azimuth analysis shows some wave polarization close to the direction of the mountain.

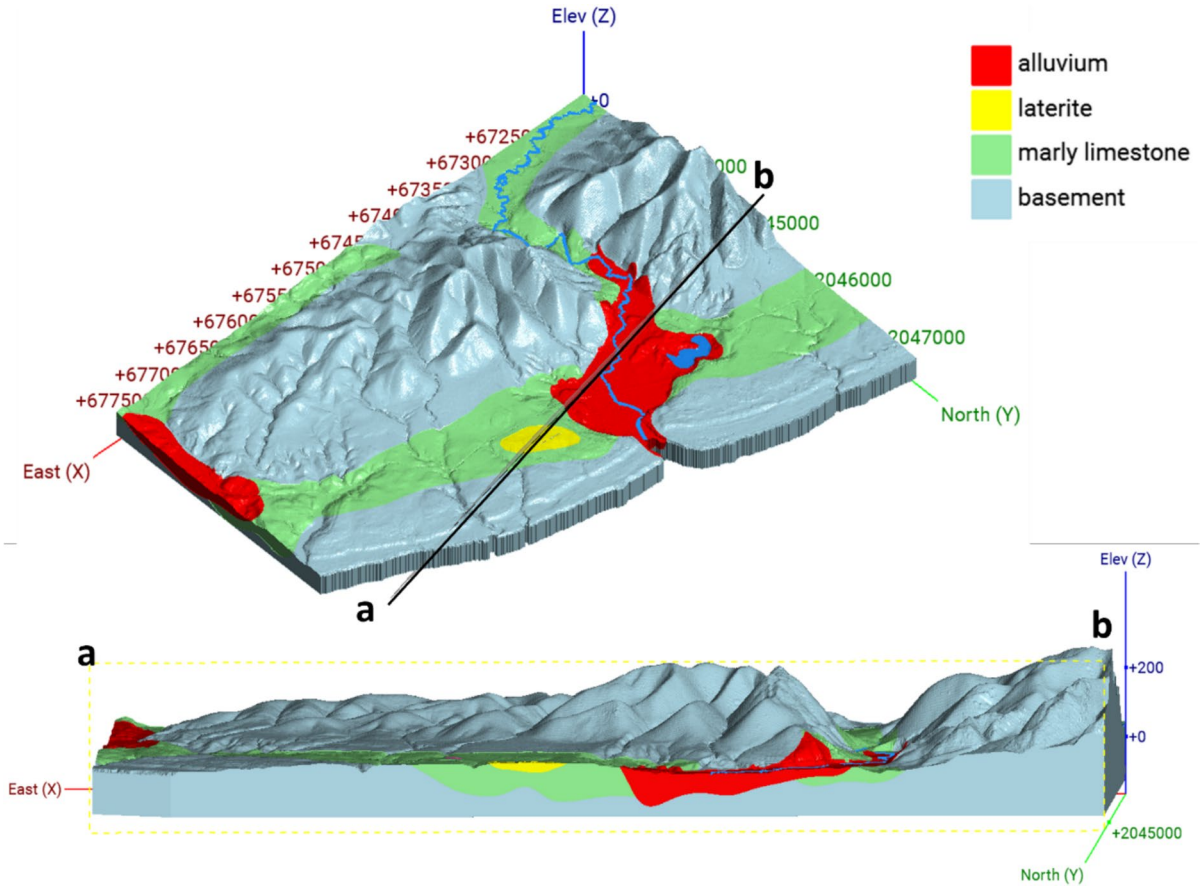

Fig. 13 The geomodel and related roughly E-W trending cross-section constructed in Leapfrog Works with input data obtained from geostatistical simulation in the R/RStudio environment. The topography is generated with a DEM of 5 m resolution in the WGS84 UTM Zone 18 CRS

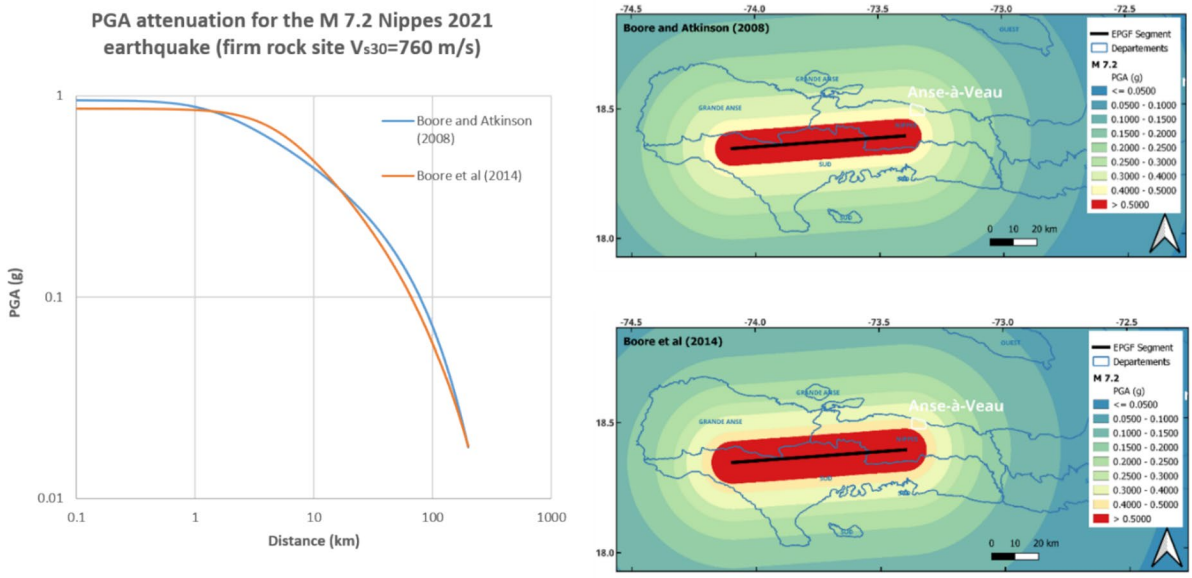

Fig. 14 Results of the seismic scenario for the M 7.2 Nippes 2021 earthquake. The maps are computed for a uniform firm rock site of V_{S30} = 760 m/s across the southern peninsula

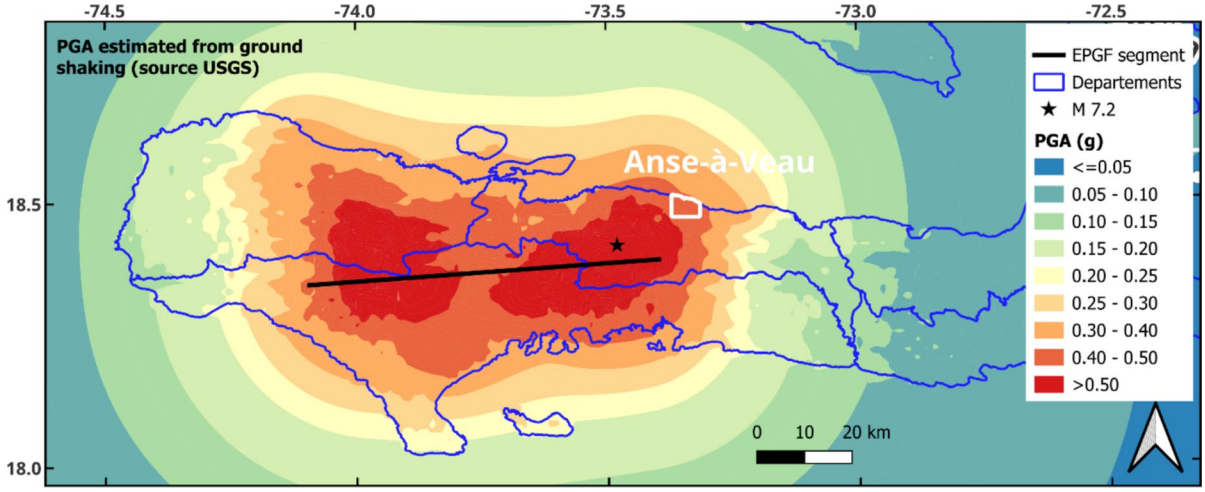

Fig. 15 Map of PGA of the southern peninsula for the M 7.2 Nippes 2021 earthquake estimated from ground shaking with data compiled by the US Geological Survey

The anisotropy shown by the geostatistical analysis indicates a more continuous behaviour of the data in the same direction, but the contrast in the variogram map is not clear enough for a reliable conclusion.

The low frequencies and high amplitude in the H/V curves are present in *La Basse Ville* and correspond to high site amplification potential. Some peaks with the higher amplitudes are also observed near the municipality of Arnaud, but they typically appear at higher frequencies. The low frequency with low-amplitude peaks in *La Haute Ville* indicate a lower site effect potential. The SSR results for the seismic station in *La Basse Ville* confirm the resonance behaviour indicated by the HVSR observed for this zone though there are some differences in the corresponding frequency peaks and amplitudes.

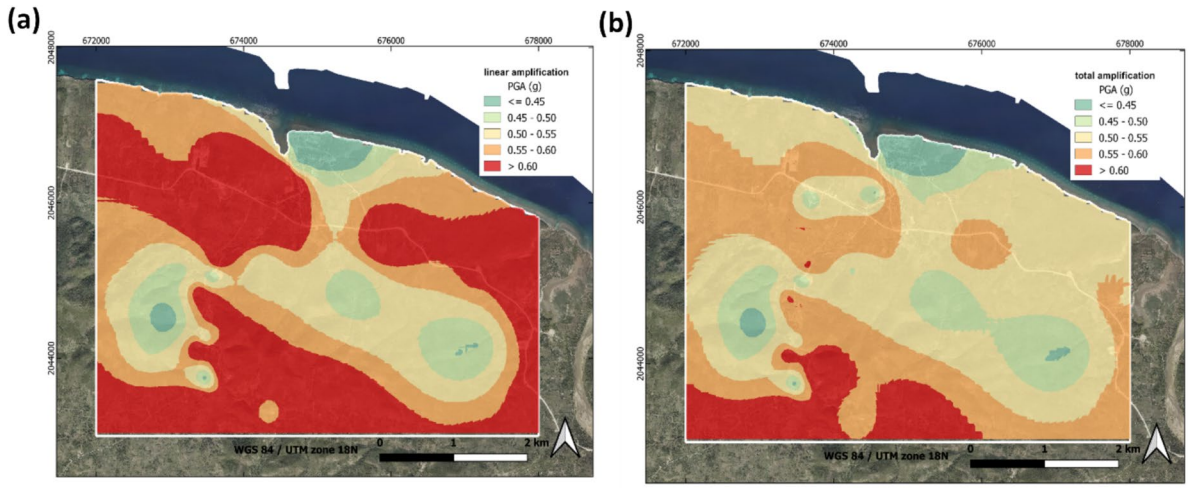

Fig. 16 PGA distribution maps for the area of Anse-à-Veau from the NGA (Boore et al. 2014). (**a**) The PGA with linear site amplification. (**b**) The PGA with total (both linear and nonlinear) site amplification

The SRT and ERT results allow the understanding of the soil properties at different depths, which helps identify areas that could amplify seismic vibrations based on their composition and compactness. They prove that low *Vp* and low resistivity values correspond to soft soil such as the alluvium formation observed in *La Basse Ville* along the river (*Rivière Brossard*). The low *Vs*, *Vp* and resistivity values found in the southern part of *La Haute Ville* correspond to the laterite observed in this zone. The H/V curves in this zone are either intermediate with no clear peak or two clear peaks curves. These conclusions are considered in the conditional simulation for the geomodelling.

The construction of the geomodel has been completed using a variogram and the conditional simulation as part of two-point geostatistics method for practical application. The NGA (Boore and Atkinson 2008; Boore et al. 2014) equation allow the estimation of the PGA distribution of the 2021 Nippes earthquake for the southern peninsula and for the area of Anse-à-Veau considering the site amplification term. In the linear domain, the PGA is high where the *Vs* value is low, but this behaviour is only observed for V_{S30} greater than 360 m/s when adding the non-linear site amplification term. This could correspond to attenuation related to non-linearity behaviour of the soft layers below 360 m/s.

The study shows that geostatistical analysis applied to geophysical data can be a very important tool to assess the depth of sedimentary deposits and enhance the geomodelling. Low *Vs* coupled with low fundamental frequency and high amplitude align with the alluvial deposits, while the high *Vs* zones show lower amplification. The integration of kriging and simulation methods for geomodelling further enhances the spatial understanding of the local seismic hazard. These results provide a detailed characterization of seismic site effects, which, when integrated with regional seismic hazard models, will support more reliable estimates of ground motion in the event of future earthquakes.

Acknowledgements This work was carried out in the framework of a PhD thesis that is part of the Belgian-Haitian collaboration project funded by the "Académie de Recherche et d'Enseignement Supérieur (ARES)". We thank the URGéo team of the Faculty of Sciences of Haiti State University for their support and collaboration as well as the team of the Georisk and Environment of the University of Liege for their assistance.

Author contribution V.D. wrote the main manuscript text and prepared the figures. All authors reviewed the manuscript.

Data availability The data belong to the University of Liege and to the State University of Haiti.

Declarations

Competing interests The authors declare no competing interests.

References

Aki K, Richards PG (2002) Quantitative seismology, 2nd edn. University Science Books, Sausalito, Calif

Ali ST, Freed AM, Calais E, Manaker DM, McCann WR (2008) Coulomb stress evolution in Northeastern Caribbean over the past 250 years due to coseismic, postseismic and interseismic deformation. Geophys J Int 174:904–918. https://doi.org/10.1111/j.1365-246x.2008.03634.x

Armstrong M, Carignan J (1997) Géostatistique linéaire: Application au domaine minier. Presses de l'Ecole des mines Print, Paris

Atkinson GM, Boore DM (2003) Empirical ground-motion relations for subduction-zone earthquakes and their application to Cascadia and other regions. Bull Seismol Soc Am 93:1703–1729. https://doi.org/10.1785/0120020156

Avalos S, Ortiz JM (2020) Multiple-point statistics: tools and methods. Comput Geosci 141:104522. https://doi.org/10.1016/j.cageo.2020.104522

Bakun WH, Flores CH, ten Brink US (2012) Significant earthquakes on the Enriquillo fault system, Hispaniola, 1500–2010: implications for seismic hazard. Bull Seismol Soc Am 102:18–30. https://doi.org/10.1785/0120110077

Bard P-Y (1999) Microtremor measurements: a tool for site effect estimation. Effects Surf Geol Seis Motion 3:1251–1279

Bard P-Y, Bouchon M (1980) The seismic response of sediment-filled valleys. Part 1. The case of incident SH waves. Bull Seismol Soc Am 70:1263–1286

Bard PY, Campillo M, Chávez-Garcia FJ, Sánchez-Sesma F (1988) The Mexico earthquake of September 19, 1985—a theoretical investigation of large- and small-scale amplification effects in the Mexico City Valley. Earthquake Spectra 4:609–633. https://doi.org/10.1193/1.1585493

Bertil D, Prépetit C, Belvaux M, Noury G, l'équipe microzonage (2013) Microzonage sismique de Port-au-Prince (Haïti): rapport de synthèse. Tech. rep., BRGM/RC-63100-FR

BME (2005) Notice explicative de la carte géologique d'Haïti au 1/250 000ème. Tech. rep., Port-au-Prince: Direction de la Géologie et des Mines

Bonnefoy-Claudet S, Cornou C, Bard P-Y, Cotton F, Moczo P, Kristek J, Fah D (2006) H/V ratio: a tool for site effects evaluation. Results from 1-D noise simulations. Geophys J Int 167:827–837. https://doi.org/10.1111/j.1365-246x.2006.03154.x

Boore DM, Atkinson GM (2008) Ground-motion prediction equations for the averagehorizontal component of PGA, PGV, and 5%-damped PSA at spectral periods between 0.01s and 10.0 s. Earthq Spectra 24:99–138. https://doi.org/10.1193/1.2830434

Boore DM, Stewart JP, Seyhan E, Atkinson GM (2014) NGA-West2 equations for predicting PGA, PGV, and 5% damped PSA for shallow crustal earthquakes. Earthq Spectra 30:1057–1085. https://doi.org/10.1193/070113eqs184m

Borcherdt RD (1970) Effects of local geology on ground motion near San Francisco Bay. Bull Seismol Soc Am 60:29–61. https://doi.org/10.1785/BSSA0600010029

Borcherdt RD, Gibbs JF (1976) Effects of local geological conditions in the San Francisco Bay region on ground motions and the intensities of the 1906 earthquake. Bull Seismol Soc Am 66:467–500. https://doi.org/10.1785/bssa0660020467

Borcherdt RD (1994) Estimates of site-dependent response spectra for design (methodology and justification). Earthquake Spectra. https://doi.org/10.1193/1.1585791

Bourennane H (1997) Etude des lois de distribution spatiale des sols de Petite Beauce. Application à la cartographie d'un horizon par couplage de méthodes morphométriques et géostatistiques. Ph.D. dissertation, Université d'Orléans

Bourges M, Mari J-L, Jeannée N (2012) A practical review of geostatistical processing applied to geophysical data: methods and applications. Geophys Prospect 60:400–412. https://doi.org/10.1111/j.1365-2478.2011.00992.x

Bowden DC, Tsai VC (2017) Earthquake ground motion amplification for surface waves. Geophys Res Lett 44:121–127. https://doi.org/10.1002/2016gl071885

Calais E, Mazabraud Y, de Lépinay BM, Mann P, Mattioli G, Jansma P (2002) Strain partitioning and fault slip rates in the northeastern Caribbean from GPS measurements. Geophys Res Lett 29:3–4. https://doi.org/10.1029/2002gl015397

Calais E, Symithe SJ, de Lépinay BM (2022a) Strain partitioning within the Caribbean-North America transform plate boundary in southern Haiti, tectonic and hazard implications. Bull Seismol Soc Am 113:131–142. https://doi.org/10.1785/0120220121

Calais E, Freed A, Mattioli G, Amelung F, Jónsson S, Jansma P, Momplaisir R (2010) Transpressional rupture of an unmapped fault during the 2010 Haiti earthquake. Nat Gesoci 3:794–799. https://doi.org/10.1038/ngeo992

Calais E, Symithe S, Monfret T, Delouis B, Lomax A, Courboulex F, Ampuero JP, Lara PE, Bletery Q, Chèze J, Peix F, Deschamps A, de Lépinay B, Raimbault B, Jolivet R, Paul S, St Fleur S, Boisson D, Fukushima Y, Duputel Z, Xu L, Meng L (2022b) Citizen seismology helps decipher the 2021 Haiti earthquake. Science 376:283–287. https://doi.org/10.1126/science.abn1045

Campbell KW, Bozorgnia Y (2008) NGA ground motion model for the geometric mean horizontal component of PGA, PGV, PGD and 5% damped linear elastic response spectra for periods ranging from 001 to 10s. Earthquake Spectra 24:139–171. https://doi.org/10.1193/1.2857546

Chatelain J-L, Guillier B, Cara F, Duval A-M, Atakan K, Bard P-Y, Team TW (2007) Evaluation of the influence of experimental conditions on H/V results from ambient noise recordings. Bull Earthq Eng 6:33–74. https://doi.org/10.1007/s10518-007-9040-7

Chauvet P (1999) Aide-mémoire de géostatistique linéaire. Presses de l'Ecole des mines, Paris

Chilès J-P, Delfiner P (2012) Geostatistics: modeling spatial uncertainty. Wiley. https://doi.org/10.1002/9781118136188

Chiou BS-J, Youngs RR (2008) An NGA model for the average horizontalcomponent of peak ground motionand response spectra. Earthq Spectra 24:173–215. https://doi.org/10.1193/1.2894832

Cressie N (2015) Statistics for spatial data (éd. Revised edition). John Wiley & Sons Inc., Hoboken, NJ

de Lépinay BM, Deschamps A, Klingelhoefer F, Mazabraud Y, Delouis B, Clouard V,... St-Louis M (2011) The 2010 Haiti earthquake: a complex fault pattern constrained by seismologic and tectonic observations. Geophys Res Lett 38. https://doi.org/10.1029/2011gl049799

de Risi R, Penna A, Simonelli AL (2019) Seismic risk at urban scale: the role of site response analysis. Soil Dyn Earthq Eng 123:320–336. https://doi.org/10.1016/j.soildyn.2019.04.011

DeMets C, Jansma PE, Mattioli GS, Dixon TH, Farina F, Bilham R, Calais Eric, Mann P (2000) GPS geodetic constraints on Caribbean-North America plate motion. Geophys Res Lett 27:437–440. https://doi.org/10.1029/1999gl005436

Douilly R, Haase JS, Ellsworth WL, Bouin M-P, Calais E, Symithe SJ, Armbruster JG, de Lepinay BM, Deschamps A, Mildor S-L, Meremonte ME, Hough SE (2013) Crustal structure and fault geometry of the 2010 Haiti earthquake from temporary seismometer deployments. Bull Seismol Soc Am 103:2305–2325. https://doi.org/10.1785/0120120303

Emery X (2012) Cokriging random fields with means related by known linear combinations. Comput Geosci 38:136–144. https://doi.org/10.1016/j.cageo.2011.06.001

Flores CH, ten Brink, U. S., Bakun WH (2012) Accounts of damage from historical earthquakes in the Northeastern Caribbean, to aid in the determination of their location and intensity magnitudes. Tech. rep., U.S. Geological Survey. https://doi.org/10.3133/ofr20111133

Frankel AD (1995) Mapping seismic hazard in the central and eastern United States. Seismol Res Lett 66:8–21. https://doi.org/10.1785/gssrl.66.4.8

Frankel A, Harmsen S, Mueller C, Calais E, Haase J (2011) Seismic hazard maps for Haiti. Earthq Spectra 27:S23–S41. https://doi.org/10.1193/1.3631016

Geli L, Bard P-Y, Jullien B (1988) The effect of topography on earthquake ground motion: a review and new results. Bull Seismol Soc Am 78:42–63. https://doi.org/10.1785/bssa0780010042

Gräler B, Pebesma E, Heuvelink G (2016) Spatio-temporal interpolation using gstat. R J 8:204–218

Hakimov F, Domej G, Ischuk A, Reicherter K, Cauchie L, Havenith H-B (2021) Site amplification analysis of Dushanbe City Area, Tajikistanto support seismic microzonation. Geosciences 11:154. https://doi.org/10.3390/geosciences11040154

Homan J, Eastwood WJ (2001) The 17 August 1999 Kocaeli (İzmit) earthquake: historical records and seismic culture. Earthq Spectra 17:617–634. https://doi.org/10.1193/1.1423654

Isaaks EH, Srivastava RM (1989) Applied geostatistics. Oxford Univ. Press, New York, NY

Journel AG, Huijbregts CJ (1978) Mining geostatistics. Academic Press. https://doi.org/10.2307/2287429

Joyner WB, Boore DM (1993) Methods for regression analysis of strong-motion data. Bull Seismol Soc Am 83:469–487. https://doi.org/10.1785/bssa0830020469

Loke MH, Barker RD (1996) Rapid least-squares inversion of apparent resistivity pseudosections using a quasi-Newton method. Geophys Prospect 44:131–152. https://doi.org/10.1111/j.1365-2478.1996.tb00142.x

Manaker DM, Calais E, Freed AM, Ali ST, Przybylski P, Mattioli G,... de Chabalier JB (2008) Interseismic plate coupling and strain partitioning in the Northeastern Caribbean. Geophys J Int. 174:889–903. https://doi.org/10.1111/j.1365-246x.2008.03819.x

Mann P, Calais E, Ruegg J-C, DeMets C, Jansma PE, Mattioli GS (2002) Oblique collision in the northeastern Caribbean from GPS measurements and geological observations. Tectonics 21:7–26. https://doi.org/10.1029/2001tc001304

Matheron G (1970) La théorie des variables regionalisées, et ses applications. Ecole des Mines de Paris

Mirowski PW, Tetzlaff DM, Davies RC, McCormick DS, Williams N, Signer C (2008) Stationarity scores on training images for multipoint geostatistics. Math Geosci. https://doi.org/10.1007/s11004-008-9194-0

Mukul M (1998) A spatial statistics approach to the quantification of finite strain variation in penetratively deformed thrust sheets: An example from the Sheeprock Thrust Sheet, Sevier Fold-and-Thrust belt, Utah. J Struct Geo 20:371–384. https://doi.org/10.1016/s0191-8141(97)00088-6

Myers DE (1989) To be or not to be... Stationary? That is the Question. Math Geol 21:347–362. https://doi.org/10.1007/bf00893695

Nakamura Y (1989) A method for dynamic characteristics estimation of subsurface using microtremor on the ground surface. Q Rep Railway Tech Res Inst 30:25–33

Nakamura Y, Saito A (1983) Estimations of seismic response characteristics and maximum acceleration of surface ground using strong motion records. Proc. of the 17th JSCE Earthquake Engineering Symposium, 25–28

Nakamura Y (2000) Clear identification of fundamental idea of Nakamura's technique and its applications. The 12th World Conf. on Earthquake Engineering, Auckland, New Zealand, 8

Nakamura Y (2009) Basic Structure of QTS (HVSR) and Examples of Applications. Dans M, Mucciarelli M, Herak & Cassidy J (Éds.), Increasing Seismic Safety by Combining Engineering Technologies and Seismological Data. Springer Netherlands. pp. 33–51. https://doi.org/10.1007/978-1-4020-9196-4_4

Oldenburg DW, Li Y (1994) Inversion of induced polarization data. Geophysics 59:1327–1341. https://doi.org/10.1190/1.1443692

Reynolds JM (1997) An introduction to applied and environmental geophysics (éd. Repr.) John Wiley & Sons Ltd, Chichester

Scherer J (1912) Great Earthquakes in the Island of Haiti. Bull Seismol Soc https://doi.org/10.1785/bssa0020030161

SESAME (2004) Guidelines for the implementation of the H/V spectral ratio technique on ambient vibrations. Measurements, processing and interpretation. Resreport, Sesame project - Deliverable D23.12–WP12. European

Commission–Research General Directorate Project No. EVG1-CT-2000-00026. https://www.earth-prints.org/handle/2122/47182

St-Fleur S, Bertrand E, Courboulex F, de Lépinay BM, Deschamps A, Hough SE, Prepetit C (2016) Site effects in Port-au-Prince (Haiti) from the analysis of spectral ratio and numerical simulations. Bull Seismol Soc Am 106:1298–1315. https://doi.org/10.1785/0120150238

Ulysse S, Boisson D, Prépetit C, Havenith H-B (2018a) Site effect assessment of the Gros-Morne Hill area in Port-au-Prince, Haiti. Part A: Geophys Seismol Surv Res Geosci 8:142. https://doi.org/10.3390/geosciences8040142

Ulysse S, Boisson D, Prépetit C, Havenith H-B (2018b) Site effect assessment of the Gros-Morne hill area in Port-au-Prince, Haiti, Part B: mapping and modelling results. Geosciences (Basel) 8:233. https://doi.org/10.3390/geosciences8070233

Ulysse S, Boisson D, Dorival V, Guerrier K, Préptit C, Cauchie L, Mreyen Anne-Sophie, Havenith H-B (2021) Site effect potential in Fond Parisien, in the east of Port-au-Prince, Haiti. Geosciences (Basel) 11:175. https://doi.org/10.3390/geosciences11040175

Wathelet M, Chatelain J-L, Cornou C, di Giulio G, Guillier B, Ohrnberger M, Savvaidis A (2020) Geopsy: a user-friendly opensource tool set for ambient vibration processing. Seismol Res Lett 91:1878–1889. https://doi.org/10.1785/0220190360

Woodring WP, Brown JS, Burbank WS (1924) Geology of the Republic of Haiti, 1st edn. Dept. Of Public Works, Port-au-Prince, Rep. of Haiti

Wu C, Wu J, Luo Y, Zhang L, Degloria SD (2009) Spatial estimation of soil total nitrogen using cokriging with predicted soil organic matter content. Soil Sci Soc Am J 73:1676–1681. https://doi.org/10.2136/sssaj2008.0205

Zhou H (2018) Review on the study of topographic effect on seismic ground motion. Earthq Sci 31:110–116. https://doi.org/10.29382/eqs-2018-0110-8